Southern African Large Telescope

High Resolution Spectrograph

SALT HRS

3210AE0034 Optical Appendix B

Stuart Barnes
University of Canterbury

Contents

Figures

This document contains a subset of:

Barnes, S. The design and performance of high resolution échelle spectrographs in astronomy, PhD Thesis, University of Canterbury, 2004.

Chapter 1

Echelle spectrograph theory

1.1 Properties of échelle gratings

1.1.1 Grating equation

A schematic of a diffraction grating is shown in Figure 1.1. A reflective surface (having a normal N) has been ruled with grooves which have spacing σ. These grooves cause the light incident at an angle α to be diffracted through an angle β. According to Huygen's principle each groove facet, which has a width σ_s, acts as a source for (plane) diffracted wavefronts. A given wavelength λ will interfere constructively only if the following condition applies:

$$m\lambda = \sigma(\sin\alpha + \sin\beta) \quad . \tag{1.1}$$

This is the classical form of the diffraction grating equation which assumes that the incident and diffracted rays are all perpendicular to the grooves. It is also possible to illuminate the grating at angle γ with respect to the facet normal (in the x-z plane, see Figure 1.2) in which case the grating equation becomes

$$m\lambda = \sigma(\sin\alpha + \sin\beta)\cos\gamma \quad . \tag{1.2}$$

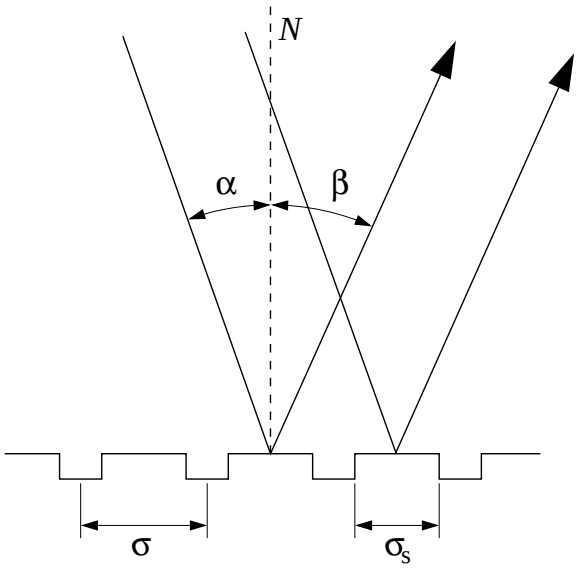

Figure 1.1: Schematic diagram of a (reflection) diffraction grating.

1.1.2 Blazed gratings

The grating can be made to diffract a high proportion of the energy into a single diffraction direction by orientating the grating facets such that a chosen wavelength (in a given

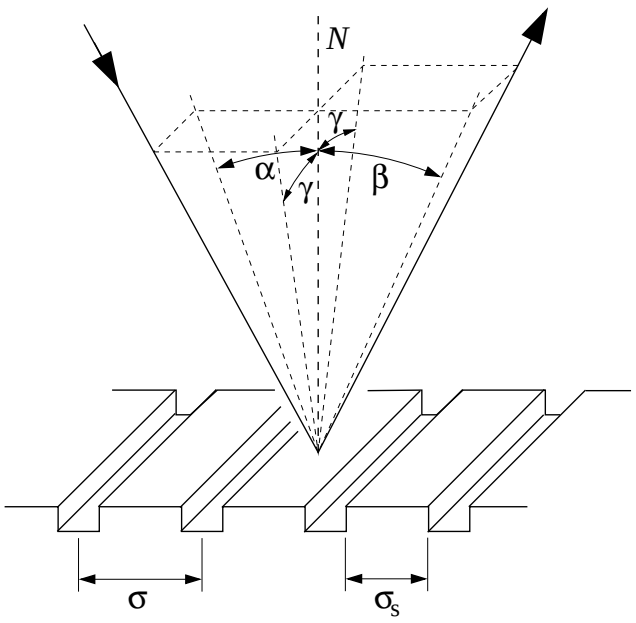

Figure 1.2: Schematic diagram of a grating where $\gamma \neq 0$.

diffraction order) is incident and diffracted at very nearly the same angle. This effect is termed blazing, and is achieved by orientating the grating facets so that the diffraction angle is very nearly same as the angle of specular reflection. As shown in Figure 1.3a, the grating facet angle with respect to the grating normal is called the blaze angle $\theta_{\rm B}$. An échelle grating is simply a standard blazed grating which has a large blaze angle. Such gratings are often referred to in terms of an "R-number" which is the tangent of the blaze angle. For instance an R2 grating has a blaze angle $\theta_{\rm B} = 63.4°$ while an R4 grating has a blaze angle $\theta_{\rm B} = 76.0°$. From Figure 1.3a it can be seen that the angles of incidence and dispersion α and $\bar{\beta}$ are related to the blaze angle $\theta_{\rm B}$ of the grating by:

$$\begin{aligned} \alpha &= \theta_{\rm B} + \theta \quad \text{and} \\ \bar{\beta} &= \theta_{\rm B} - \theta \quad , \end{aligned} \tag{1.3}$$

where θ is the facet illumination angle with respect to the facet normal. That is $\bar{\beta}$ is the angle of diffraction for a wavelength $\lambda_{\rm B}$ (the blaze wavelength) in the centre of order m. Echelle gratings can also be illuminated out of the normal plane (see Figure 1.3b) and it follows that the blaze wavelength $\lambda_{\rm B}$ is defined in terms of the grating equation (equation 1.2) as

$$\begin{aligned} m\lambda_{\rm B} &= \sigma(\sin\alpha + \sin\bar{\beta})\cos\gamma \\ &= 2\sigma \sin\theta_{\rm B}\cos\theta\cos\gamma \quad . \end{aligned} \tag{1.4}$$

For reasons of efficiency the only viable modes in which an échelle grating can be operated are where $\alpha > \bar{\beta}$ or that $\alpha \approx \bar{\beta}$ (see Schroeder and Hilliard, 1980 and Section 1.1.11). The situation where $\theta = 0$ (i.e., $\alpha = \bar{\beta}$) is termed the Littrow condition and if $\gamma \neq 0$ the condition becomes quasi-Littrow. Under Littrow illumination, the optical step of a grating $\sigma_{\rm t}$ is given by

$$\sigma_{\rm t} = \sigma \sin\theta_{\rm B} \quad , \tag{1.5}$$

and the facet width is

$$\sigma_{\rm s} = \sigma \cos\theta_{\rm B} \quad . \tag{1.6}$$

This determines the order of interference for diffracted light. That is,

$$m = \frac{2\sigma_{\mathrm{t}}}{\lambda} \quad . \tag{1.7}$$

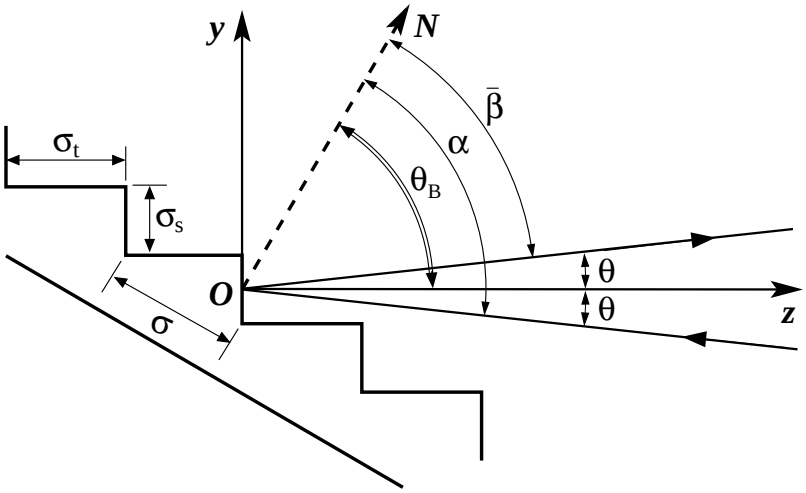

(a) Profile of échelle grating.

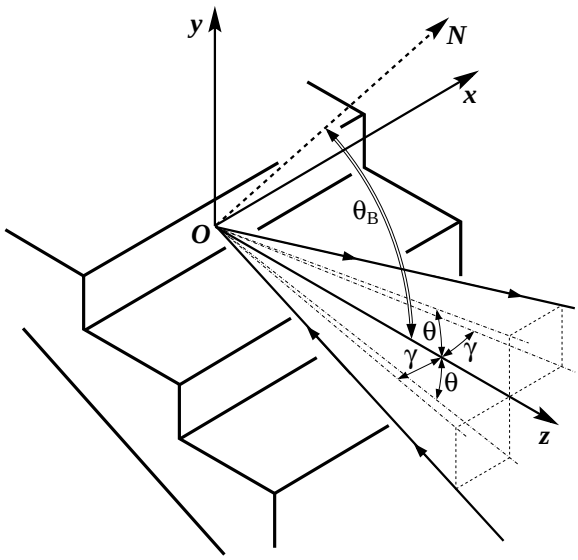

(b) Isometric view of échelle grating.

Figure 1.3: Schematic diagram of an échelle grating. The definitions of the blaze angle θ_{B}, angle of incidence α and the angle of diffraction β are shown in (a). The angle $\bar{\beta}$ is the angle of diffraction in the centre of each order m. The facet illumination angle θ is defined with respect to the facet normal O-z. All these angles are defined in the y-z plane. The definition of γ is shown in (b). It is the angle of incidence with respect to the facet normal as measured in the x-z plane.

1.1.3 Angular and linear dispersion

The angular dispersion of a grating is found by differentiating equation 1.2 with respect to λ for a given α. This gives

$$\frac{\mathrm{d}\beta}{\mathrm{d}\lambda} = \frac{m}{\sigma \cos\beta \cos\gamma} \quad , \tag{1.8}$$

or

$$\frac{\mathrm{d}\beta}{\mathrm{d}\lambda} = \frac{\sin\alpha + \sin\beta}{\lambda \cos\beta} \quad , \tag{1.9}$$

which in the centre of an order, at the blaze wavelength, becomes

$$\frac{\mathrm{d}\beta}{\mathrm{d}\lambda} = \frac{2 \sin\theta_\mathrm{B} \cos\theta}{\lambda_\mathrm{B} \cos\bar{\beta}} \quad . \tag{1.10}$$

From these equations it can be seen that for a given wavelength high angular dispersion can be obtained either by making α (and β) large or by increasing the grating groove density (i.e., small σ). Echelle gratings make use of this fact by having large blaze angles and by being coarsely ruled. Typical échelle gratings have from 30 to 300 grooves mm^{-1}) and they therefore operate with large values of m (i.e., $m = 10$ to > 100).

The angular dispersion is independent of the optical system of which the grating is part. The linear dispersion is determines the extent δl of a spectral region $\delta\lambda$ on a given detector and is given by

$$\delta l = f_\mathrm{cam} \frac{\mathrm{d}\beta}{\mathrm{d}\lambda} \delta\lambda \quad , \tag{1.11}$$

where f_cam is the focal length of the camera used to image the spectrum. The plate factor P is the reciprocal linear dispersion and is therefore

$$P = \left(f_\mathrm{cam} \frac{\mathrm{d}\beta}{\mathrm{d}\lambda} \right)^{-1} \quad . \tag{1.12}$$

1.1.4 Free spectral range

The free spectral range $\Delta\lambda_\mathrm{FSR}$ is defined as the change in wavelength from an order m to the next $(m \pm 1)$. Any wavelength that appears in an order m will also appear in orders $m-1$ and $m+1$; however the angle of diffraction will be quite different as will the diffracted intensity. The free spectral range is given by

$$\Delta\lambda_\mathrm{FSR} = \frac{\lambda}{m}, \tag{1.13}$$

which in terms of the blaze wavelength, λ_B, becomes

$$\begin{aligned} \Delta\lambda_\mathrm{FSR} &= \frac{\lambda_\mathrm{B}^2 \cos\gamma}{2\sigma \sin\theta_\mathrm{B} \cos\theta} \\ &\approx \frac{\lambda_\mathrm{B}^2}{2t} \quad . \end{aligned} \tag{1.14}$$

The angular extent of one free spectral range is determined by multiplying the free spectral range (equation 1.13) with the angular dispersion (equation 1.8). That is,

$$\begin{aligned} \Delta\beta_{\mathrm{FSR}} &= \frac{\mathrm{d}\beta}{\mathrm{d}\lambda}\Delta\lambda_{\mathrm{FSR}} \\ &= \frac{\lambda_{\mathrm{B}}}{\sigma\cos\bar{\beta}\cos\gamma} \quad , \end{aligned} \tag{1.15}$$

which, if $\theta = 0$, becomes $\Delta\beta_{\mathrm{FSR}} = \lambda_{\mathrm{B}}/(\sigma_{\mathrm{s}}\cos\gamma)$. This is simply diffraction from a rectangular slit of width σ_{s}. The diffraction pattern has an angular width $\lambda/\sigma_{\mathrm{s}}$. From the above equations it can be seen that for a given diffraction angle β and order number m both the angular extent of an échelle spectrum depends largely on the density of the échelle rulings. A coarsely ruled grating (large σ) will produce a spectrum with a smaller angular extent (per free spectral range) than a more finely ruled grating.

1.1.5 Anamorphic magnification

If a source is of angular distance $\delta\alpha$ as viewed from the grating then after dispersion it will have an angular separation $\delta\beta$, where

$$\delta\beta = \delta\alpha\frac{\mathrm{d}\beta}{\mathrm{d}\alpha} \quad . \tag{1.16}$$

Now, from equation 1.1, it is straight-forward to show that

$$r = \left|\frac{\mathrm{d}\beta}{\mathrm{d}\alpha}\right| = \frac{\cos\alpha}{\cos\beta} \quad . \tag{1.17}$$

The quantity $r = \cos\alpha/\cos\beta$ is called the anamorphic magnification. The effect of anamorphic magnification on the dispersed light from an échelle grating is illustrated in Figure 1.4. It can be shown that a beam with a diameter B which is incident on a grating at angle α will after diffraction through an angle β have a diameter B' given by

$$B' = \frac{B}{r} \quad . \tag{1.18}$$

It should be noted that the anamorphic magnification can vary considerably across a single free spectra range. This is particularly significant for high R-number gratings, which generally have a larger angular free spectral range.

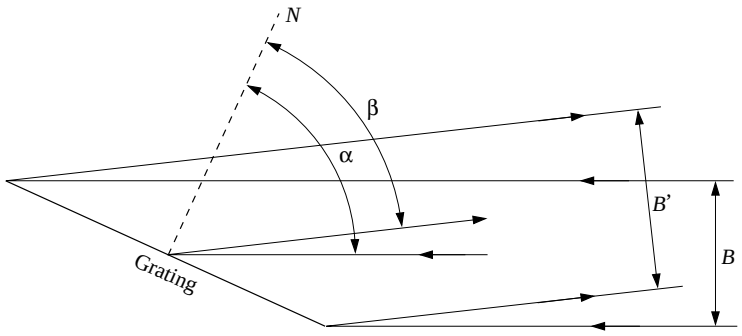

Figure 1.4: The effect of anamorphic magnification on beam size.

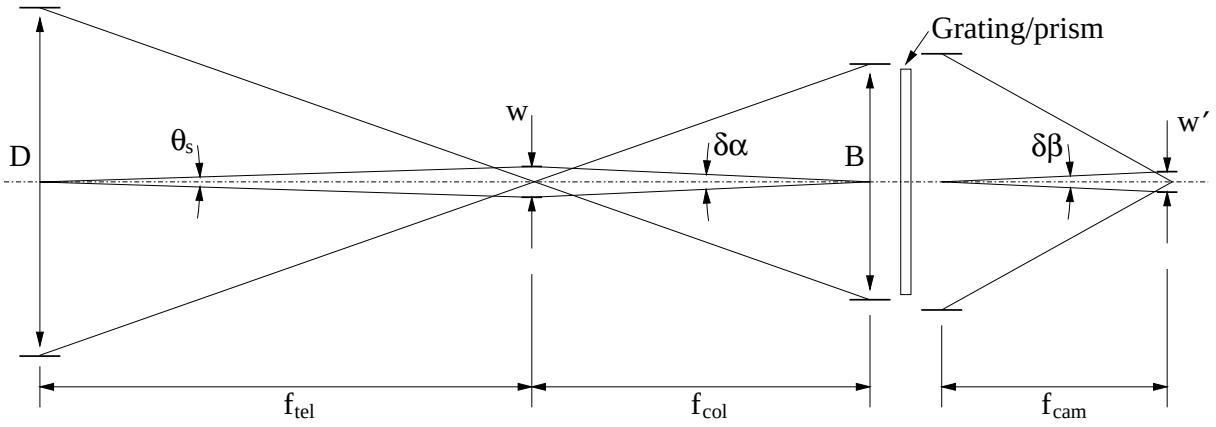

Figure 1.5: Schematic diagram of a slit limited a spectrograph (after Schroeder, 2000).

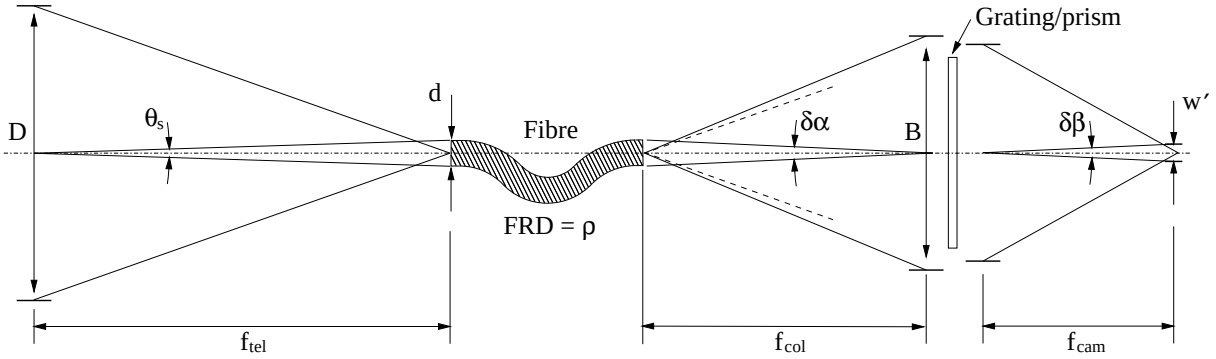

Figure 1.6: Schematic diagram of a fibre-fed spectrograph. The cone of light which exits the fibre is slightly larger than would be expected in the absence of a fibre (dashed line).

1.1.6 Direct and fibre spectrographs

A schematic slit-limited spectrograph is shown in Figure 1.5. A telescope of diameter D and focal length $f_{\rm tel}$ feeds a spectrograph which has an entrance slit width w. The fibre-fed spectrograph (Figure 1.6) is identical to the directly fed spectrograph except that a fibre of diameter d replaces the slit. In both cases the angle subtended by the slit or fibre on the sky is

$$\begin{aligned} \theta_{\rm s} &= \frac{w}{f_{\rm tel}} \quad \text{or} \\ \theta_{\rm s} &= \frac{d}{f_{\rm tel}} \quad . \end{aligned} \tag{1.19}$$

If the spectrograph is directly coupled to the telescope (for instance, in coudé, Cassegrain or Nasmyth configurations) then the following equality will apply:

$$\frac{f_{\rm tel}}{D} = \frac{f_{\rm col}}{B} \quad , \tag{1.20}$$

where $f_{\rm col}$ is the focal length of the collimator. If instead the spectrograph is coupled to a telescope via an optical fibre then after the light has passed through the fibre it will

emerge with an output focal ratio $F_{\rm out}$ which is faster than the input focal ratio $F_{\rm in}$, where

$$F_{\rm in} = \frac{f_{\rm tel}}{D} \quad \text{and} \quad F_{\rm out} = \frac{f_{\rm col}}{B} \quad . \tag{1.21}$$

This effect is known as focal ratio degradation (FRD, see for example Angel, 1977 or Ramsey, 1988) can be described in terms of a FRD parameter ρ:

$$\rho = \frac{F_{\rm out}}{F_{\rm in}} \quad . \tag{1.22}$$

Although FRD always has the effect of decreasing the focal ratio, the amount by which it is decreased depends upon the focal ratio at which the fibre is fed. A typical fibre fed at an optimal focal ratio will decrease the focal ratio by about 10% to 20% (i.e., $\rho = 1.1$ to 1.2). Now, because of FRD, the equality given in equation 1.20 becomes for fibre-fed instruments

$$\frac{f_{\rm tel}}{D} = \rho \frac{f_{\rm col}}{B} \quad . \tag{1.23}$$

That is, in order for the beam size to remain constant on the same spectrograph which is first directly fed and then later fibre-fed, the focal length of the collimator must be reduced. In order to preserve throughput, the effective resolving power will thereby be reduced (see Section 1.1.10) which justifies this effect being termed a degradation. The use of fibres for spectroscopy will also be briefly discussed in Section 1.2.4.

1.1.7 Slit width and height

As viewed from the grating, the angular size of the slit is $\delta\alpha = w/f_{\rm col}$ or $\delta\alpha = d/f_{\rm col}$. It was shown above that this slit will undergo anamorphic magnification and therefore the image of this slit will have a width w' given by

$$\begin{aligned} w' &= w\frac{f_{\rm cam}}{f_{\rm col}} r \quad \text{or} \\ &= d\frac{f_{\rm cam}}{f_{\rm col}} r \quad . \end{aligned} \tag{1.24}$$

The slit height h' will be

$$\begin{aligned} h' &= h\frac{f_{\rm cam}}{f_{\rm col}} r' \quad \text{or} \\ &= d\frac{f_{\rm cam}}{f_{\rm col}} r' \quad , \end{aligned} \tag{1.25}$$

where r' is the anamorphic magnification introduced by the cross-disperser. This is generally (but not always) negligible.

1.1.8 Line tilt

Although the quasi-Littrow mode of grating illumination offers advantages in terms of efficiency, a non-zero γ has the effect of tilting the slit image with respect to the direction of dispersion. Due to the finite height of the slit, there is a small change in the angle of incidence with respect to the facet normal (in the x-z plane) from the bottom of the slit to the top. As shown in Figure 1.7, if the change in γ is $\delta\gamma$, then there will be a corresponding change in the angle of diffraction, $\delta\beta$, which will result in a line tilt ϕ given by

$$\tan\phi = \frac{\delta\beta}{\delta\gamma} = \frac{\mathrm{d}\beta}{\mathrm{d}\gamma} \quad , \tag{1.26}$$

where it should be noted that $\delta\beta/\delta\gamma$ is not necessarily a constant, and hence the tilt angle ϕ will vary across the slit image height. This line curvature will only be noticeable for very long slit heights. It follows that

$$\frac{\mathrm{d}\beta}{\mathrm{d}\gamma} = \frac{\mathrm{d}\beta}{\mathrm{d}\lambda}\,\frac{\mathrm{d}\lambda}{\mathrm{d}\gamma} \quad , \tag{1.27}$$

where $\mathrm{d}\beta/\mathrm{d}\lambda$ is the échelle angular dispersion (equation 1.8 or 1.9) and from the grating equation

$$\frac{\mathrm{d}\lambda}{\mathrm{d}\gamma} = -\frac{\sigma}{m}(\sin\alpha + \sin\beta)\sin\gamma \quad . \tag{1.28}$$

Therefore

$$\begin{aligned} \tan\phi &= \frac{\sin\alpha + \sin\beta}{\cos\beta}\,\frac{\sin\gamma}{\cos\gamma} \\ &= \lambda\frac{\mathrm{d}\beta}{\mathrm{d}\lambda}\tan\gamma \quad , \end{aligned} \tag{1.29}$$

which at the blaze wavelength λ_B the line tilt becomes

$$\tan\phi = 2\tan\theta_\mathrm{B}\tan\gamma \quad . \tag{1.30}$$

Note that from equation 1.30 it can be seen that high R-number gratings are more susceptible to line tilt. It is also significant to note that if some of the cross-dispersive power occurs before the échelle grating then the line tilt will have a wavelength dependence.

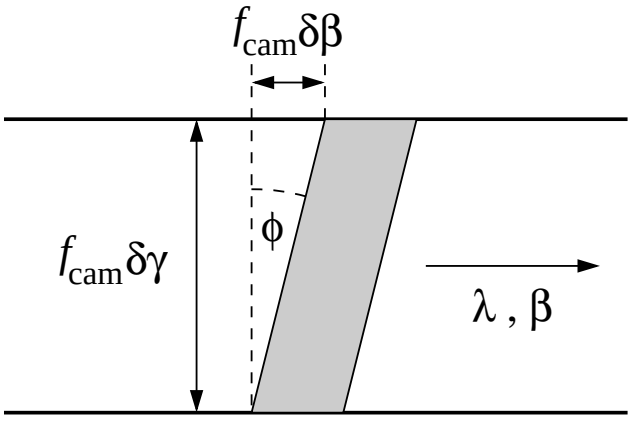

Figure 1.7: Schematic of a tilted slit image. This is due to the finite height of the slit which slightly changes γ.

Fibre tilt

The effect of line tilt on a fibre requires more detailed consideration. As before, a non-zero γ will tilt the dispersed fibre image by an amount ϕ given by equation 1.29. This tilt will however simply shear the fibre in the direction of échelle dispersion (see Figure 1.8). A detailed schematic of this sheared fibre is shown in Figure 1.9. The unsheared image of the fibre is an ellipse (due to anamorphic magnification of the circular fibre) which has a height h and width w. This ellipse has an equation

$$\frac{4x^2}{w^2} + \frac{4y^2}{h^2} = 1 \quad , \quad \text{or} \quad h'^2x^2 + w^2y^2 - \frac{w^2h^2}{4} = 0 \quad . \tag{1.31}$$

The ellipse is then sheared through an angle ϕ giving

$$\begin{aligned} x' &= x + y\tan\phi \quad \text{and} \\ y' &= y \quad , \end{aligned} \tag{1.32}$$

which if substituted into equation 1.31 gives

$$x'^2 - 2\tan\phi\, x'y' + \left(\tan^2\phi + \frac{w^2}{h^2}\right)y'^2 - \frac{w^2}{4} = 0 \quad . \tag{1.33}$$

Equation 1.33 can be recognized as a quadratic equation of the form

$$A'x'^2 + B'x'y' + C'y'^2 + F' = 0 \quad , \tag{1.34}$$

where the coefficients are

$$\begin{aligned} A' &= 1 \quad , \\ B' &= -2\tan\phi \quad , \\ C' &= \tan^2\phi + \frac{w^2}{h^2} \quad \text{and} \\ F' &= -\frac{w^2}{4} \quad . \end{aligned} \tag{1.35}$$

Because the discriminant $B'^2 - 4A'C' = -4\frac{w^2}{h^2} < 0$ this sheared ellipse is also an ellipse. However, the major axis of this ellipse does not form an angle ϕ to the major axis of the unsheared ellipse. In fact, it can be shown that the sheared ellipse is equivalent to an ellipse of the form

$$A''x''^2 + C''y''^2 + F'' = 0 \quad , \tag{1.36}$$

which has been rotated through an angle ϕ_e given by

$$\begin{aligned} \cot 2\phi_e &= \frac{A' - C'}{B'} \\ &= \frac{1}{2\tan\phi}\left(\tan^2\phi + \frac{w^2}{h^2} - 1\right) \\ &= \frac{1}{2}\frac{w^2}{h^2}\cot\phi - \cot 2\phi \quad . \end{aligned} \tag{1.37}$$

The coefficients of the unrotated ellipse are

$$\begin{aligned} A'' &= A' \cos^2 \phi_e + B' \cos \phi_e \sin \phi_e + C' \sin^2 \phi_e \quad , \\ C'' &= A' \sin^2 \phi_e - B' \sin \phi_e \cos \phi_e + C' \cos^2 \phi_e \quad \text{and} \\ F'' &= F' \quad . \end{aligned} \tag{1.38}$$

Now, if equation 1.36 is rewritten in the form

$$\frac{x''^2}{a^2} + \frac{y''^2}{b^2} = 1 \quad , \tag{1.39}$$

we find that the major and minor axis lengths a and b are given by

$$a^2 = \frac{-F''}{A''} \quad \text{and} \quad b^2 = \frac{-F''}{C''} \quad . \tag{1.40}$$

The full width w_e of the sheared ellipse is given by

$$\frac{w_e}{2} = x_e + y_e \tan \phi \quad , \tag{1.41}$$

and can be derived by noting that at $(x, y) = (x_e, y_e)$

$$\frac{\mathrm{d}y}{\mathrm{d}x} = -\cot \phi \quad . \tag{1.42}$$

Given that in polar coordinates

$$x = \frac{w}{2} \cos \theta \quad \text{and} \quad y = \frac{h}{2} \sin \theta \tag{1.43}$$

it is straightforward to show that

$$w_e = w \sec \phi_e \quad , \tag{1.44}$$

where

$$\tan \phi_e = \tan \left(\frac{h}{w} \tan \phi \right) \quad . \tag{1.45}$$

The relevance of the above derivation will become apparent when the resolving power of fibre-fed échelle spectrographs is considered below (Section 1.1.10).

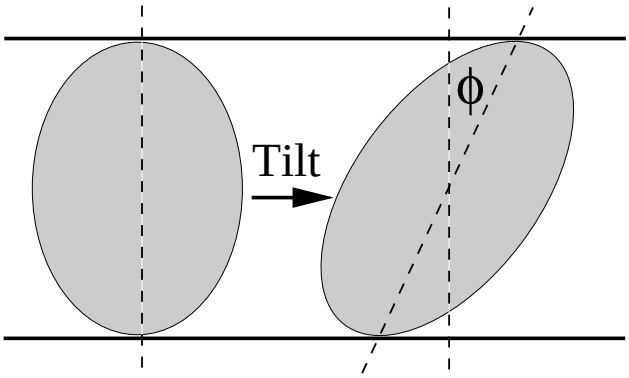

Figure 1.8: A fibre image sheared by line tilt.

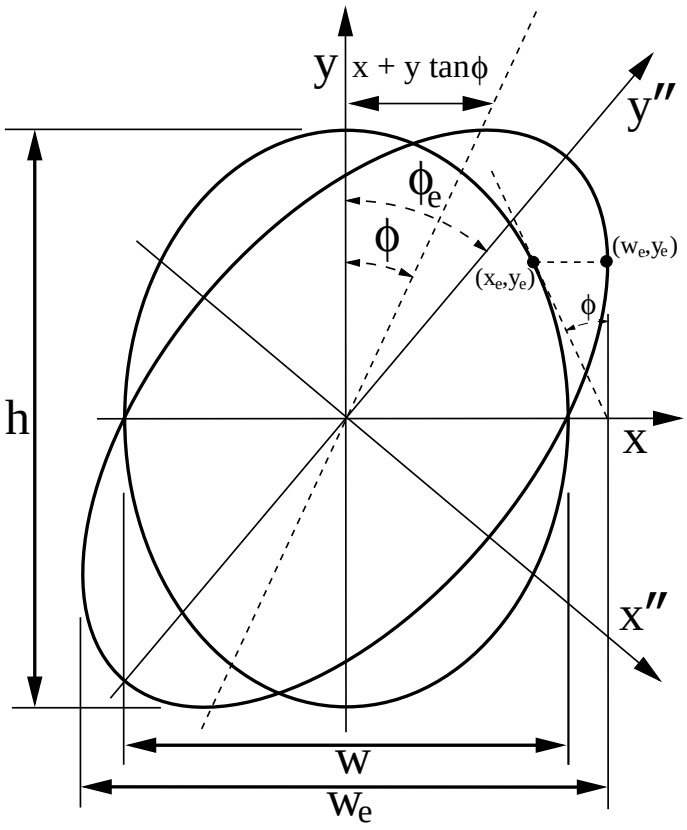

Figure 1.9: Schematic of a tilted fibre. The fibre image has been sheared by line tilt through an angle ϕ. The sheared image is an ellipse with axes which have been rotated through an angle ϕ_e. See text for details.

1.1.9 Cross dispersion

Because échelle gratings generally work at relatively high order numbers (i.e, $m \gg 1$) there are many combinations of m and λ that satisfy the grating equation. Therefore, an échelle grating will usually be used in conjunction with a second dispersive element which will disperse the spectra in a direction that is orthogonal to the main échelle dispersion. This element could be either a grating or a prism (or a combination of the two; for instance, a grism). This is shown schematically in Figure 1.10. It would also be possible to separate the orders by using a filter which is tuned to allow transmittance of only one free spectral range centred on the wavelength of interest. However, this would negate one of the most attractive features of an échelle spectrograph. That is, if the order separation is done by an element with low dispersive power it is possible to arrange many orders into a 2-dimensional format which can be simultaneously imaged by a single camera. The choice of cross-dispersers will be discussed further in Section 1.2.2.

Order separation

If the spectrograph camera has a focal length $f_{\rm cam}$, then the separation between orders will be

$$\Delta y = f_{\rm cam} \frac{{\rm d}\beta}{{\rm d}\lambda}_{\rm XD} \Delta\lambda_{\rm FSR} \quad , \tag{1.46}$$

where ${\rm d}\beta/{\rm d}\lambda_{\rm XD}$ is the angular dispersion of the cross-disperser. If we express the free spectral range in terms of the blaze wavelength $\lambda_{\rm B}$ then equation 1.46 becomes

$$\Delta y = f_{\rm cam} \frac{{\rm d}\beta}{{\rm d}\lambda}_{\rm XD} \frac{\lambda_{\rm B}^2}{2\sigma \sin\theta_{\rm B} \cos\theta} \quad . \tag{1.47}$$

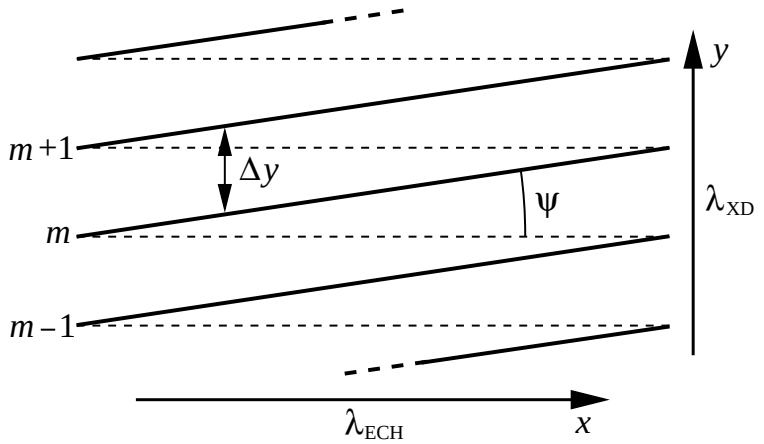

Figure 1.10: Schematic of échelle cross-dispersion.

Order tilt and curvature

As shown in Figure 1.10 the orders will be tilted by an amount ψ. The angle ψ is given by

$$\tan\psi = \frac{{\rm d}\beta/{\rm d}\lambda_{\rm XD}}{{\rm d}\beta/{\rm d}\lambda_{\rm ECH}} \quad , \tag{1.48}$$

where $\mathrm{d}\beta/\mathrm{d}\lambda_{\mathrm{ECH}}$ is the angular dispersion of the échelle grating and $\mathrm{d}\beta/\mathrm{d}\lambda_{\mathrm{XD}}$ is the angular cross dispersion. In the order centre the tilt is

$$\tan\psi_{\mathrm{B}} = \frac{\mathrm{d}\beta}{\mathrm{d}\lambda}_{\mathrm{XD}} \frac{\lambda\cos\bar{\beta}}{2\sin\theta_{\mathrm{B}}\cos\theta} \quad . \tag{1.49}$$

However, because the échelle angular dispersion is not completely uniform throughout an individual order (i.e, equations 1.8 and 1.9) the orders will be slightly curved.

1.1.10 Resolving power

If a spectrograph has marginally sufficient resolution to distinguish between two wavelengths λ_1 and $\lambda_2 = \lambda_1 + \delta\lambda$ then the resolving power is defined as

$$R = \frac{\lambda}{\delta\lambda}, \tag{1.50}$$

where $\lambda \approx \lambda_1 \approx \lambda_2$. The angular width between the two wavelengths λ_1 and λ_2 in the dispersed beam will be $\delta\beta$, so in terms of the angular dispersion $(\mathrm{d}\beta/\mathrm{d}\lambda)$, equation 1.50 may be written as

$$R = \frac{\lambda}{\delta\beta}\frac{\mathrm{d}\beta}{\mathrm{d}\lambda} \quad . \tag{1.51}$$

Now, from equation 1.16 the above becomes

$$R = \frac{\lambda}{\delta\alpha}\frac{\mathrm{d}\alpha}{\mathrm{d}\lambda} \quad . \tag{1.52}$$

The resolving power may now be written in a more useful form by noting that

$$\frac{\mathrm{d}\alpha}{\mathrm{d}\lambda} = \frac{\sin\alpha + \sin\beta}{\lambda\cos\alpha} \quad , \tag{1.53}$$

which gives

$$\begin{aligned} R &= \frac{1}{\delta\alpha}\frac{\sin\alpha + \sin\beta}{\cos\alpha} \\ &= \frac{1}{\delta\alpha}\frac{2\tan\theta_\mathrm{B}}{(1 - \tan\theta_\mathrm{B}\tan\theta)} \quad . \end{aligned} \tag{1.54}$$

The term $\cos\gamma$ is ignored here as γ is always small and therefore $\cos\gamma \approx 1$.

Diffraction limit

The diffraction limited resolving power can be derived from equation 1.54 by noting that,

$$m\lambda = \frac{L}{N}(\sin\alpha + \sin\beta) \quad , \tag{1.55}$$

where N is the number of grooves across a grating which has a length L. If the collimated beam size is B, then it follows that $B = L\cos\alpha$ and that the diffraction limited angular slit size $\delta\alpha$ is approximately λ/B (or, equivalently $\theta_\mathrm{s} \approx \lambda/D$). Therefore, in the diffraction limit,

$$R = mN \quad . \tag{1.56}$$

Directly fed spectrographs

In the case of a directly fed spectrograph equation 1.54 becomes

$$R = \frac{f_\mathrm{col}}{w}\frac{2\tan\theta_\mathrm{B}}{(1 - \tan\theta_\mathrm{B}\tan\theta)} \quad . \tag{1.57}$$

Combining equations 1.57, 1.19 and 1.20 gives

$$R = \frac{2B \tan \theta_{\rm B}}{\theta_{\rm s} D (1 - \tan \theta_{\rm B} \tan \theta)} \quad . \tag{1.58}$$

This provides a very useful way of determining the resolving power of a spectrograph in terms of the diameter and focal length of the telescope, the slit width (expressed in terms of the angle the slit subtends on the sky), and the size of the collimated beam which is incident on the spectrograph's grating. If the collimated beam can be matched to the projected length of the échelle grating (i.e., $B = L \cos \alpha$) then equation 1.58 can be rewritten as

$$R = \frac{2L \sin \theta_{\rm B} \cos \theta}{\theta_{\rm s} D} \quad . \tag{1.59}$$

This equation was first given by Bingham (1979).

What these equations (1.58 and 1.59) show is that in order to obtain a large resolving power with a given slit size it is necessary either to have a large grating size or a large collimated beam (i.e., large L or B). This was the solution for the large coudé spectrographs used from 1910 to 1980. Equation 1.58 shows the merit of the échelle solution; that is, to use large $\theta_{\rm B}$. However, as shown by equation 1.59, the usefulness of increasing the blaze angle is not without limits; that is, for R2 gratings, $\sin \theta_{\rm B} = 0.89$ while for R4 $\sin \theta_{\rm B} = 0.97$. Also, if the dimensions of the collimated beam are such that $B > L \cos \alpha$ then equation 1.58 is more appropriate. As will be shown (Section 1.1.12) although the overfilled grating will result in the loss of light, it is still possible to improve the overall throughput of the spectrograph for a given product of R and $\theta_{\rm s}$.

Fibre-fed spectrographs

The effect of FRD has been described in Section 1.1.6. The FRD term ρ modifies the resolving power of a fibre-fed spectrograph to

$$R = \frac{2B \tan \theta_{\rm B}}{\rho \theta_{\rm s} D (1 - \tan \theta_{\rm B} \tan \theta)} \quad \text{and} \tag{1.60}$$

$$R = \frac{2L \sin \theta_{\rm B} \cos \theta}{\rho \theta_{\rm s} D} \quad . \tag{1.61}$$

It is relevant to note that because the FRD of a given fibre depends only on the input focal ratio, this is the only means by which the focal ratio of the telescope can effect the resolving power of a fibre-fed spectrograph.

Effective fibre resolving power

The resolving power of a slit limited spectrograph will be given by equations 1.58 and 1.59 only if the seeing disk is considerably larger that the slit width, thereby providing a uniformly illuminated rectangle. If the seeing disk only partially fills the spectrograph's entrance slit, or if the entrance slit is entirely absent, then the resolving power equations must be somewhat modified. This will not be discussed here. However, for a discussion see Schroeder (2000, pp 318–320).

The entrance slit if a fibre is always circular and essentially uniform in surface brightness. The effective resolving power R' of a circular fibre of diameter d can be calculated

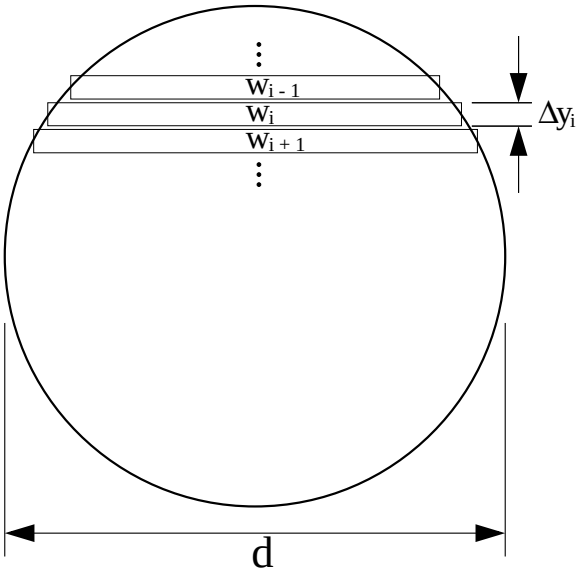

Figure 1.11: The flux weighted fibre width is calculated by weighting each chord by the area it encompasses.

by subdividing the fibre into many narrow slits which have widths $w_{\rm i}$ equal to the chord which is parallel to the direction of dispersion. This is shown in Figure 1.11. Each slit will then have a weighting which equals the fraction of the total flux which the slit encloses. This fraction is proportional to the area of each slit, where the normalized area $A_{\rm i}$ of each slit is

$$A_{\rm i} = \frac{w_{\rm i}\Delta y_{\rm i}}{\pi\frac{d^2}{4}} \quad . \tag{1.62}$$

Therefore, the flux weighted fibre width is given by

$$\bar{w} = \sum_{\rm i=1}^{\rm n} w_{\rm i} A_{\rm i} \quad , \tag{1.63}$$

In the limit where $n \rightarrow \infty$ $\Delta y_{\rm i} \rightarrow {\rm d}y$ and $A_{\rm i} \rightarrow w{\rm d}y$ equation 1.63 can be solved to give

$$\bar{w} = \frac{8}{3\pi}\, d \quad . \tag{1.64}$$

This factor was first derived by Vaughnn (1994), although he gave an expression for the flux-weighted slit width of a fibre which has been reimaged onto a slit which is smaller than the fibre diameter (or alternatively, the slit could be imprinted directly on the fibre exit face). If the slit width is $w_{\rm s}$ the flux-weighted slit width becomes

$$\bar{w} = \frac{8}{3\pi}\, d \left(1 - \left(1 - \left(\frac{w_{\rm s}}{d} \right)^2 \right)^{3/2} \right) \frac{1}{T} \quad , \tag{1.65}$$

where the relative transmission T of the clipped fibre is given by

$$T = 1 + \frac{2}{\pi} \left(\frac{w_{\rm s}}{d} \left(1 - \left(\frac{w_{\rm s}}{d} \right)^2 \right)^{1/2} - \cos\left(\frac{w_{\rm s}}{d} \right) \right) \quad . \tag{1.66}$$

Obviously, if $w_s = d$, $T = 1$, and $\bar{w} = 8\,/\,3\pi\,d$. Hence, the effective resolving power of a (fully illuminated) fibre is

$$\begin{aligned} R' &= \frac{d}{\bar{w}}\,R \\ &= \frac{3\pi}{8}\,R \\ &\approx \frac{R}{0.849} \quad . \end{aligned} \tag{1.67}$$

While the above shows that a fibre will deliver a resolving power that is considerably better than the resolving power that can be achieved with a uniformly illuminated slit with a width equal to the diameter of the fibre, the convention is to measure the full-width at half-maximum (FWHM) of a monochromatic light source which can be either a single laser line or the emission lines formed by an appropriate calibration light source. This method makes the assumption that the profile of a single line, after extraction to one-dimension (hereinafter called the line-spread function, or LSF) can be approximated by a gaussian. In fact, as will be shown below, this will not be the case, and the resolving power measured by this method will be quite different from that derived above.

The extracted profile (or LSF) of a fibre image can be determined by noting that the extraction in one dimension of an elliptical fibre image produces another ellipse which will have a normalized height of one and a minor-axis equal to the fibre image width w. That is, the equation of an extracted fibre will be:

$$I_{\rm fib} = \sqrt{1 - \frac{4x^2}{w^2}} \quad , \qquad \frac{-w}{2} < x < \frac{w}{2} \quad . \tag{1.68}$$

In order to approximate the observed fibre profile $I_{\rm obs}$ the extracted profile is then convolved with a one-dimensional point-spread function (PSF); i.e.,

$$I_{\rm obs} = I_{\rm fib} \otimes I_{\rm psf} \quad . \tag{1.69}$$

The effect of the PSF will depend on the image quality that the spectrograph produces. To show how image quality affects the final line profile gaussians with FWHMs which varied in proportion to the fibre image width were used. The FWHM of the PSF varied from $w_{\rm psf} = 0.1w$ to $w_{\rm psf} = 0.5w$. The changing ratio can be used to represent either a change in image quality or a change in the size of the fibre image.

The FWHM of the fibre profiles can now be determined by fitting a gaussian to the extracted and convolved fibre profile. It appears reasonable to insist that the fitted gaussian is normalized to have the same equivalent width as the fibre profile, although in practice this makes little difference to the parameters of the fitted gaussian (assuming both width and height are variables). The results are shown in Figure 1.12. The fibre profiles determined using this method are shown in Figure 1.13. It is noted that the fit to a gaussian is very poor when the effect of the PSF is small, although as the relative effect of the PSF increases the approximation by a gaussian becomes more appropriate. The limit of the FWHM as $w_{\rm psf} \rightarrow 0$ is $w_{\rm fwhm} = 0.682w$. Hence, if the spectrograph has perfect optics, the resolving power would be measured as

$$R(w_{\rm psf} = 0) \approx \frac{R}{0.682} \quad , \tag{1.70}$$

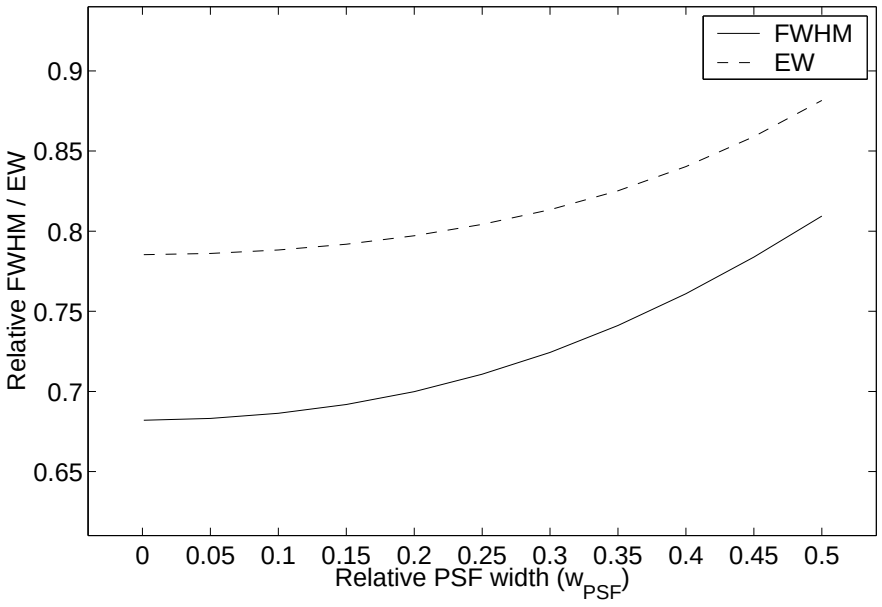

Figure 1.12: The FWHM of synthetic fibre profiles. Normalized gaussians were fitted to the profiles shown in Figure 1.13 in order to obtain the FWHM. Equivalent widths of the fibre profiles are shown for comparison.

and to a good approximation, the resolving power as a function of $w_{\rm psf}$ is given by

$$R(w_{\rm psf}) \approx \frac{R(w_{\rm psf}=0)}{\sqrt{1+1.6\,w_{\rm psf}^2}} \quad . \tag{1.71}$$

In practice, the optics of the spectrograph (as well as the properties of the CCD) will tend to degrade the resolving power. If a degradation in resolving power (which is measured using the above method) due to optical performance of 10% is acceptable, then the FWHM of the PSF should be no more than $0.35 \rightarrow 0.40 \times w$.

Effect of line tilt

As described in Section 1.1.8 the effect of a non-zero γ will be to tilt the dispersed slit image by an amount ϕ given by equation 1.27. This will have the effect of decreasing the resolving power. In the case of a slit spectrograph it may be possible to counter-rotate the slit in order to minimize this tilt, although as pointed out by Schroeder and Hilliard (Schroeder and Hilliard, 1980) the throughput-resolution product remains constant.

The entrance slit of a fibre-fed spectrograph cannot however be rotated. It will be stated without proof that the extracted profile of a tilted fibre is simply equation 1.68 where the fibre image width w is replaced by the full-width $w_{\rm e}$ of the tilted fibre (equation 1.44). Hence, the extracted profile of a tilted fibre will be given by

$$I' = \sqrt{1-\frac{4x^2}{{w_{\rm e}}^2}} \quad , \qquad \frac{-w_{\rm e}}{2} < x < \frac{w_{\rm e}}{2} \quad . \tag{1.72}$$

The observed fibre profile can now be obtained by convolving equation 1.72 with a one-dimensional PSF. As above, the FWHM of this profile can be measured. This is shown in Figure 1.14 and the measured equivalent widths are shown in Figure 1.15.

The relative change in FWHM is shown in Figure 1.16. It can be seen that as image

quality becomes worse the relative effect of line tilt decreases. If, for a given image quality the resolving power at zero line tilt is $R'(\phi = 0)$ (see equation 1.71) then the resolving power as a function of line tilt is given by

$$R'(\phi) = R'(\phi = 0)\frac{w}{w_{\mathrm{e}}} \quad . \tag{1.73}$$

In the small angle approximation this reduces to

$$R'(\phi) = \frac{R'(\phi = 0)}{\sqrt{1 + \frac{h^2}{w^2}\phi^2}} \quad , \tag{1.74}$$

where it should be noted that the fibre image height h must also be considered. Hence, in order for line tilt to degrade the resolving power by less than 10% it can be seen that a line tilt of up to $\phi \approx 20^\circ$ can be tolerated.

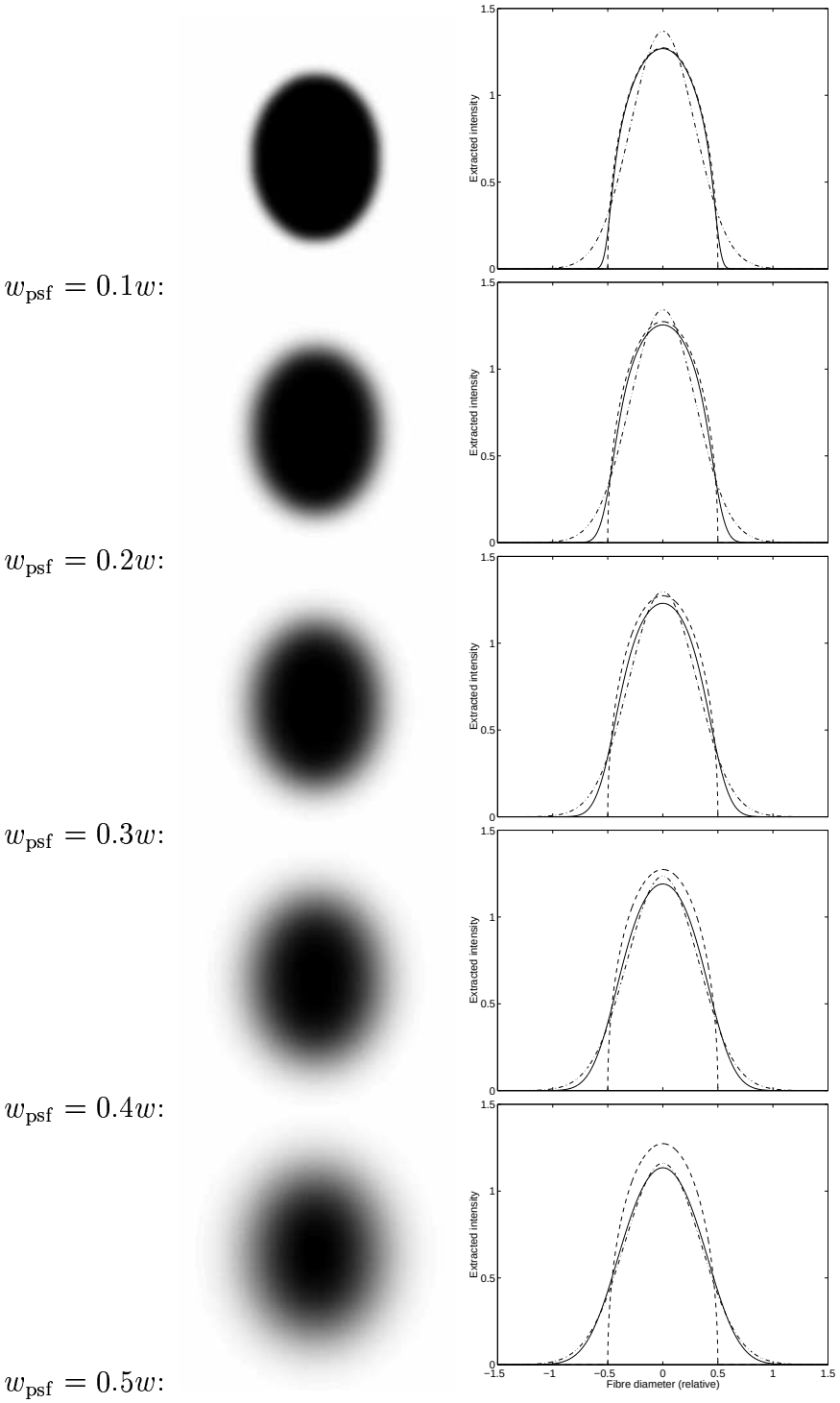

Figure 1.13: Synthetic fibre images and profiles. The output from a circular fibre has been convolved with a gaussian PSF (left). The PSF's have a FWHM ranging from 0.1 to 0.5 times the fibre image width w. The extracted profile (bold) is then normalized and fitted by a gaussian (dot-dashed). Note that the unconvolved fibre profile (dotted) is well approximated by a gaussian only when the influence of the PSF is large.

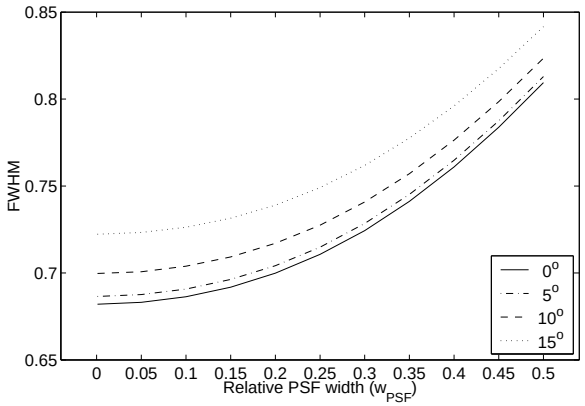

Figure 1.14: The FWHM of extracted and tilted fibre profiles.

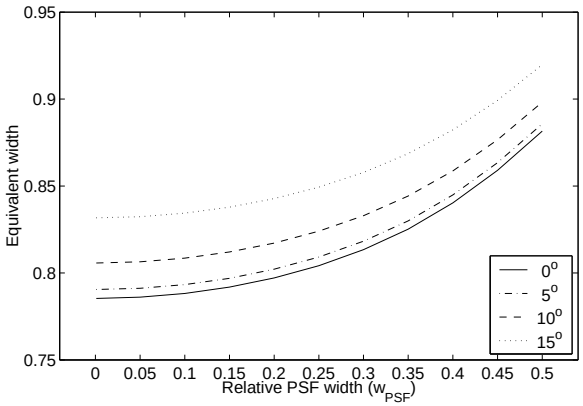

Figure 1.15: The equivalent width of extracted and tilted fibre profiles.

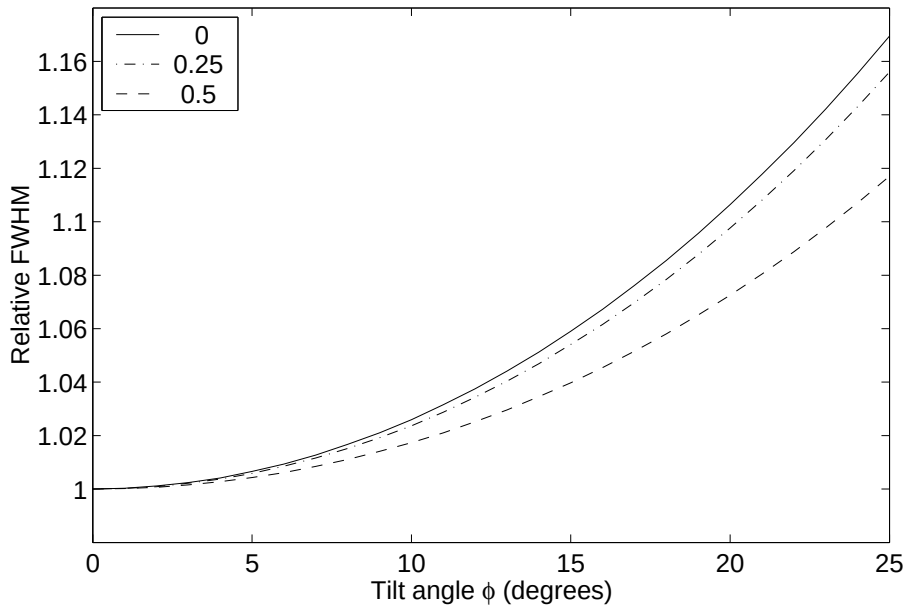

Figure 1.16: The relative FWHM of extracted and tilted fibre profiles.

Total resolving power

The above equations (equations 1.58, 1.59, 1.60 and 1.61) give only the slit or fibre limited resolving power of a given spectrograph. The total effective resolving power will however be degraded by several additional factors; for example by imperfect optics and detectors. If these degrading factors can each be assigned to resolving power influences $R_{\rm i}$, then the total resolving power of the spectrograph $R_{\rm tot}$ will be given by,

$$\frac{1}{R_{\rm tot}^2} = \sum_{\rm i=1}^{\rm n} \frac{1}{R_{\rm i}^2} \quad , \tag{1.75}$$

where it is assumed that each factor can be modeled by a guassian function with a FWHM given by $R_{\rm i}$. Some of the contributors to the total resolving power include the following:

- the diffraction limited resolving power given by $R_{\rm dif} = mN$, where N is the total number of grooves being illuminated. The diffraction limit will invariably be somewhat degraded by imperfections in the grating surface; for instance, surface irregularities and groove ruling errors.

- optical aberrations. The use of imperfect optics, even if they are diffraction limited, is unavoidable.

- detector properties. These include the effects of the depletion layer and charge migration in silicon detectors. The effects of finite pixel sampling must also be considered.

The optical quality and detector properties must therefore be chosen in order to ensure that the degradation is acceptable. While all of the above influences are unavoidable, there may be other transient effects such as focus errors or image motion which will further degrade the image quality of the spectrograph. The design of the spectrograph should attempt to mitigate all such effects.

1.1.11 Efficiency

Upon striking a grating at an angle α a collimated beam will be diffracted through an angle β, which depends on the wavelength λ and the grating groove spacing σ according to the grating equation (equation 1.1.1). The intensity I of this diffracted beam results from the combination of an interference function (IF) and a blaze function (BF); that is,

$$I = IF \times BF \quad . \tag{1.76}$$

The interference function that results from a grating which has a total of N equally spaced grooves is given by

$$IF = \left(\frac{\sin N\nu'}{N \sin \nu'} \right)^2 \quad , \tag{1.77}$$

where $2\nu'$ is the phase difference between rays diffracted off the centres of adjacent grooves. The blaze function is given by

$$BF = \left(\frac{\sin \nu}{\nu} \right)^2 \quad , \tag{1.78}$$

where ν is the phase difference between the centre and edge of an individual groove. These phase differences are given by

$$2\nu' = \frac{2\pi\sigma}{\lambda}(\sin\alpha + \sin\beta) \quad , \quad \text{and} \tag{1.79}$$

$$\nu = \frac{\pi\sigma_s}{\lambda}(\sin\alpha + \sin\beta) \quad . \tag{1.80}$$

Each individual grating facet has a width σ_s which may be smaller than the groove spacing σ in which case the blaze function will be broadened.

The diffracted intensity pattern for a single wavelength is shown in Figure 1.17. It

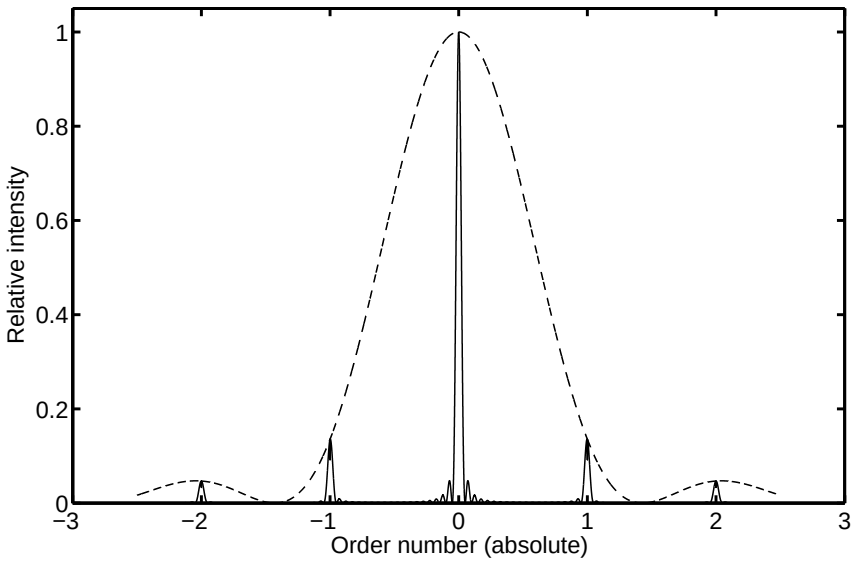

Figure 1.17: The diffracted intensity of a single wavelength (solid line). The blaze function (dashed line) modulates the interference function, which is maximum when the order number m is an integer. The intensity in diffracted orders ($m \neq 0$) is low.

can be seen that the majority of the energy incident on the grating is returned in the zeroth order ($m = 0$) where it is simply reflected. Only a small portion of the energy is diffracted into other orders.

Blaze function

The purpose of blazing a grating is to shift the blaze function so that the maximum diffracted intensity of a given wavelength coincides with chosen diffraction order. The phase difference between successive grooves (equation 1.80) is now given by

$$\nu = \frac{\pi\sigma'_{\rm s}}{\lambda}\big(\sin(\alpha-\theta_{\rm B})+\sin(\beta-\theta_{\rm B})\big) \quad , \tag{1.81}$$

where $\sigma'_{\rm s}$ is the effective size of each facet (see Figure 1.18). The effective facet size (when $\alpha > \beta$ is

$$\sigma'_{\rm s} = \frac{\sigma\cos\alpha}{\cos\theta} \quad , \tag{1.82}$$

which should be compared to the size of a clear facet $\sigma_{\rm s}$, which is $\sigma_{\rm s} = \sigma\cos\theta_{\rm B}$.

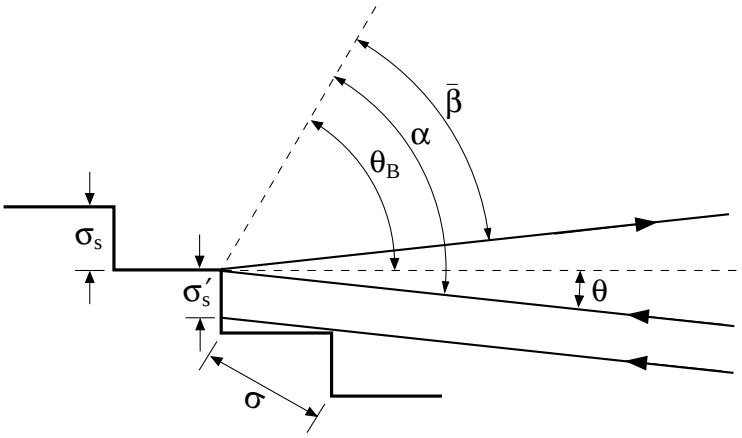

Figure 1.18: The effective facet size of a blazed grating is reduced because of shadowing (after Schroeder, 2000).

The normalized intensity of a wavelength diffracted by a grating blazed at $\theta_{\rm B} = 63.5°$ is shown in Figure 1.19. The wavelength has been chosen so that it coincides with the maximum of the blaze function which occurs in order $m = 40$.

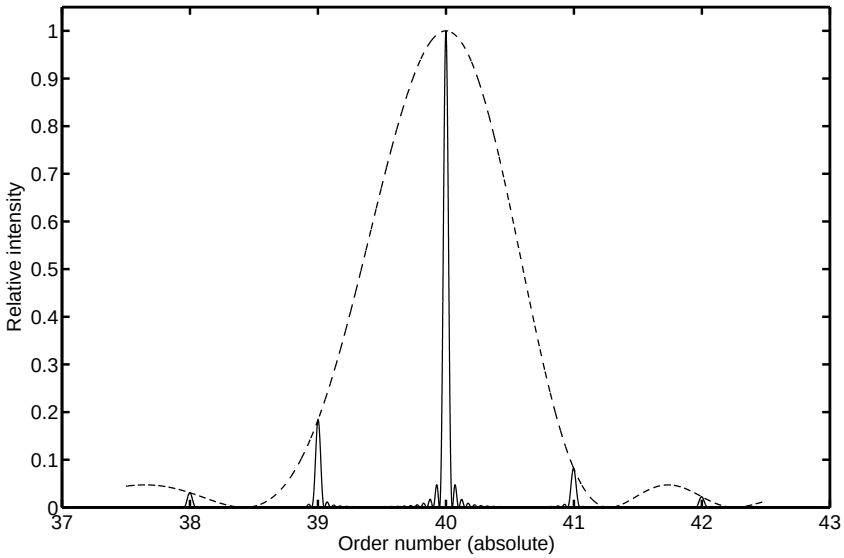

Figure 1.19: The diffracted intensity of a single wavelength using blazed grating. The blaze function is now centred on an order $m \neq 0$. Compare with Figure 1.17.

Absolute efficiency

In order to calculate the efficiency of an échelle grating it is necessary to determine the distribution of light of a given wavelength across all possible orders. A wavelength that is not at the centre of the blaze function will have a significant fraction of its energy diffracted into other orders. This is shown in Figure 1.20. The method prescribed by

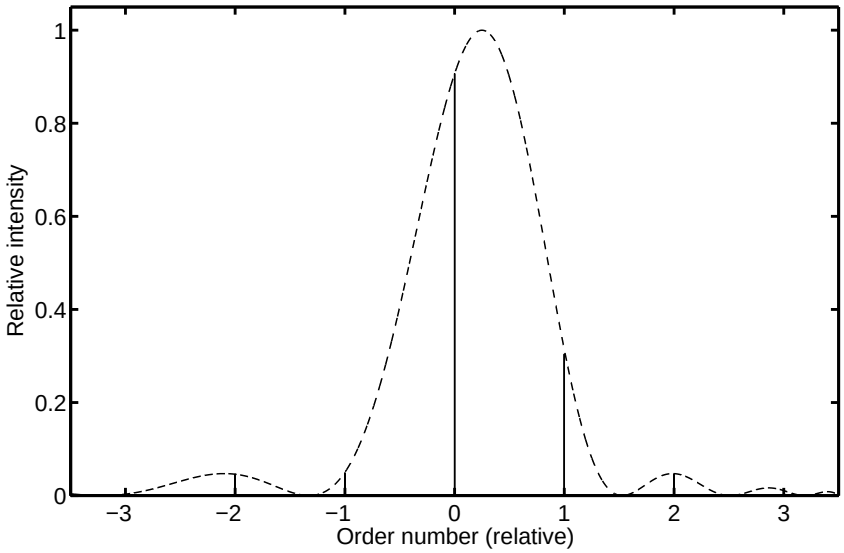

Figure 1.20: A method for computing the efficiency of an échelle grating. See text for details.

Schroeder and Hilliard (1980) is simply to sum the intensities across all possible orders and then derive the fraction that remains in the order of interest. However, as commented by Bottema (1981), this definition of efficiency is not quite correct, although it is conceded that in most cases of interest the results will be correct (Schroeder, 1981). Therefore, the absolute diffractive efficiency of an échelle grating for a wavelength in order m is

$$T_{\text{ech}} = \frac{I_{\Delta m=0}}{I_{\Delta m=0} + \sum_{\Delta m \neq 0} I_{\Delta m}} \quad , \tag{1.83}$$

where Δm and I are the relative order number and intensity respectively.

The relative efficiency of an échelle grating which is blazed at $\theta_{\text{B}} = 63^\circ$ is shown in Figure 1.21. This grating is illuminated at $\theta = 0^\circ$, which means that the wavelength free spectral range is equal to the FWHM of the blaze function. If the grating is illuminated in a non-Littrow mode ($\theta \neq 0$) then the fraction of the blaze function that is covered by one free spectral range is increased by a factor $\cos\beta / \cos\alpha$; that is

$$\Delta\lambda_{\text{FWHM}} = \frac{\Delta\lambda_{\text{FSR}}}{r} \quad , \tag{1.84}$$

where r is the anamorphic magnification. The blaze function for a range of Littrow angles (θ), such that $1.0 < 1/r < 1.5$ is shown in Figure 1.22. Note that the values of r refers to the order centre only.

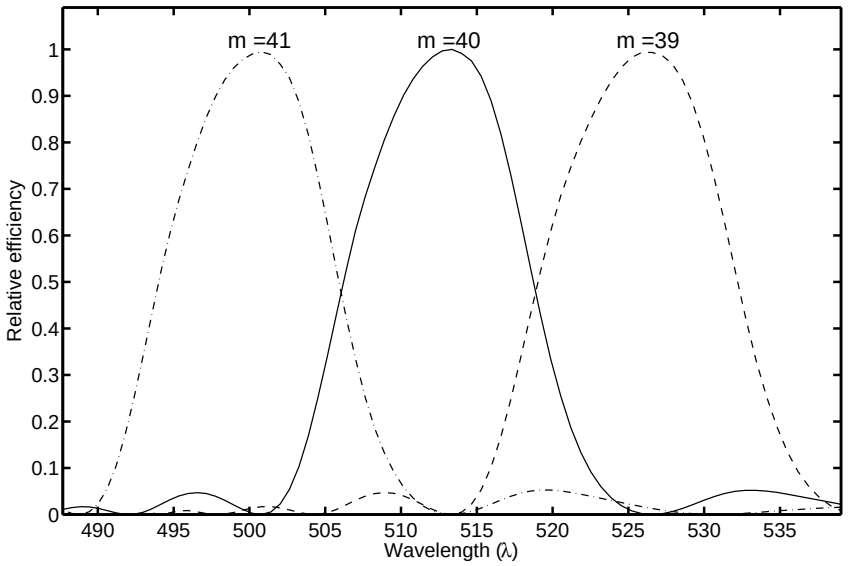

Figure 1.21: Relative efficiency of an échelle grating which is blazed at $\theta_B = 63°$.

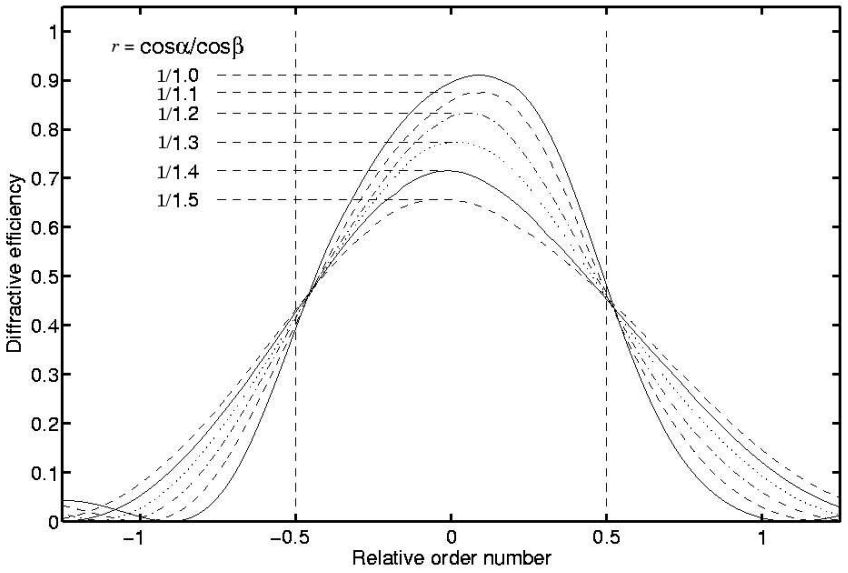

Figure 1.22: Blaze function for a range of Littrow angles (θ).

1.1.12 Overfilling

Although it has been assumed thus far that the collimated beam is matched to the projected size of the échelle grating, it is not always possible to do this. As shown in Figure 1.23, the amount by which a grating is overfilled is a function of the size of the grating (W and L) and the angle of illumination (α). Depending on the size of the grating, the

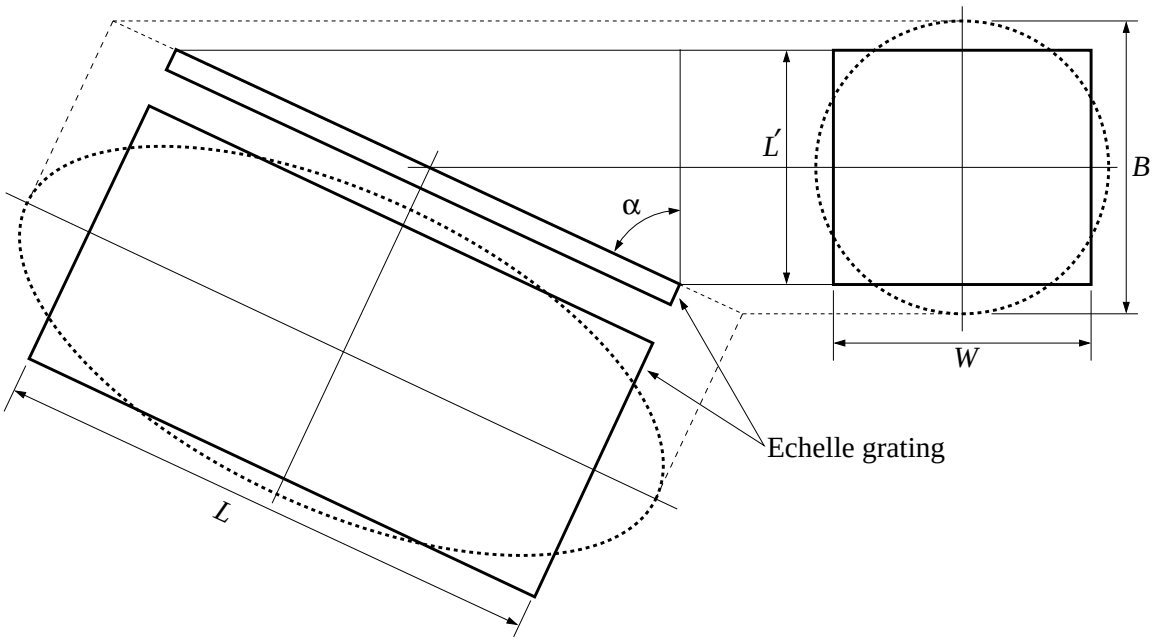

Figure 1.23: The overfilling of an échelle grating. The collimated beam, which has a diameter B, projects to an ellipse on the échelle grating (width W, length L). This projects to a height $L' = L\cos\alpha$ in the collimated beam.

elliptical footprint of the collimated beam may overfill the grating either perpendicular or parallel to the direction of the rulings (or both, as shown in Figure 1.23). If, as is shown in Figures 1.24a and 1.24b, we consider the overfilling in each of the directions separately then the fraction F of a collimated beam that is incident on a grating is given by

$$F = F_{\mathrm{W}} + F_{\mathrm{L}} - 1 \quad , \tag{1.85}$$

where F_{W} and F_{L} are the fractions of the beam captured when the overfilling in the parallel and perpendicular directions respectively. Once the grating has been projected into the collimated beam these fractions may be calculated by integrating the equation of a circle, with appropriate limits. That is,

$$F_{\mathrm{W}} = \frac{16}{\pi B^2}\int_0^{W/2}\sqrt{\frac{B^2}{4} - x}\,\mathrm{d}x \quad , \tag{1.86}$$

$$F_{\mathrm{L}} = \frac{16}{\pi B^2}\int_0^{L'/2}\sqrt{\frac{B^2}{4} - x}\,\mathrm{d}x \quad . \tag{1.87}$$

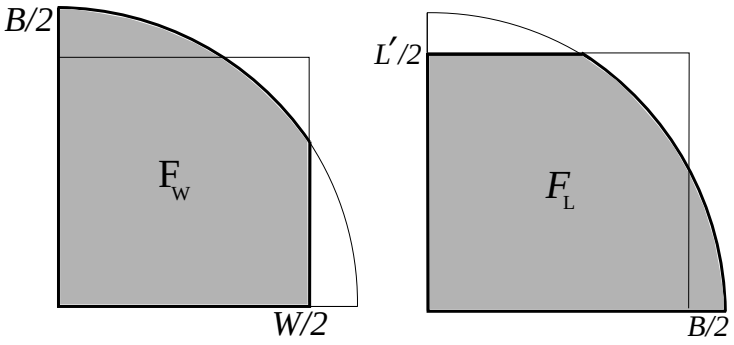

(a) W (b) L

Figure 1.24: The grating may be overfilled parallel and perpendicular to the rulings. The fraction F of the collimated beam that is incident on the échelle grating may be computed by considering the amount the grating is overfilled parallel ($F_{\rm W}$) and perpendicular ($F_{\rm L}$) to the ruling separately. See text for details.

In polar coordinates, these equations become

$$F_{\rm W} = \frac{4}{\pi}\int_{\theta_{\rm W}}^{\pi/2} \sin^2\theta \, {\rm d}\theta \quad , \tag{1.88}$$

$$F_{\rm L} = \frac{4}{\pi}\int_{\theta_{\rm L}}^{\pi/2} \sin^2\theta \, {\rm d}\theta \quad , \tag{1.89}$$

where the polar angle limits $\theta_{\rm W}$ and $\theta_{\rm L}$ are given by

$$\cos\theta_{\rm W} = \frac{W}{B} \quad \text{and} \quad \cos\theta_{\rm L} = \frac{L'}{B} \quad . \tag{1.90}$$

Evaluating equations 1.88 and 1.89 gives

$$F_{\rm W} = \frac{4}{\pi}\left[\frac{\pi}{4} - \frac{1}{2}\theta_{\rm W} + \frac{1}{4}\sin 2\theta_{\rm W}\right] \quad , \tag{1.91}$$

$$F_{\rm L} = \frac{4}{\pi}\left[\frac{\pi}{4} - \frac{1}{2}\theta_{\rm L} + \frac{1}{4}\sin 2\theta_{\rm L}\right] \quad . \tag{1.92}$$

If $W > B$, and/or $L' > B$, then the grating is not overfilled (or overfilled in one direction only) and consequently either $\theta_{\rm W} = 0$ or $\theta_{\rm L} = 0$. Hence, either $F_{\rm W} = 1$ or $F_{\rm L} = 1$ depending on the direction of overfilling.

1.2 Design of échelle spectrographs

1.2.1 Choice of échelle

The choice of grating is one of the most fundamental choices in the design of an échelle spectrograph. In the following sections some factors which influence this choice will be discussed.

Beam size

For a given échelle grating with a blaze angle θ_B which is used to obtain a given resolving power R it is not necessarily the case that the ideal beam width will be the width of the échelle grating W. It has been pointed out by Diego and Walker (1985) (see also Walker and Diego, 1985) that the échelle grating may be considerably overfilled without compromising throughput. This is because while the grating becomes less efficient as the beam size increases (due to overfilled light being lost) the angular size of the slit on the sky can be increased in order to maintain a constant resolving power.

The effect is illustrated in Figures 1.25a and 1.25b. Here an R2 échelle with $W \times L = 300 \times 840\,\mathrm{mm}$ is illuminated (in Littrow configuration) by a beam which can vary in diameter. This is done in practice by varying the telescope focal ratio. The angular slit width is varied so that a constant resolving power of $R = 25\,000$ is maintained at all beam sizes. The efficiency of the grating is therefore a function of both beam size and seeing. Figure 1.25b shows the throughput relative to a beam size of 300 mm. For small seeing values it can be seen that increasing the beam size leads to rapidly decreasing throughput as the slit throughput always remains high. However, at larger values of seeing, the throughput of the spectrograph actually increases as the beam size is increased. This is because the overfilling of the échelle becomes increasingly mitigated by the larger angular slit width.

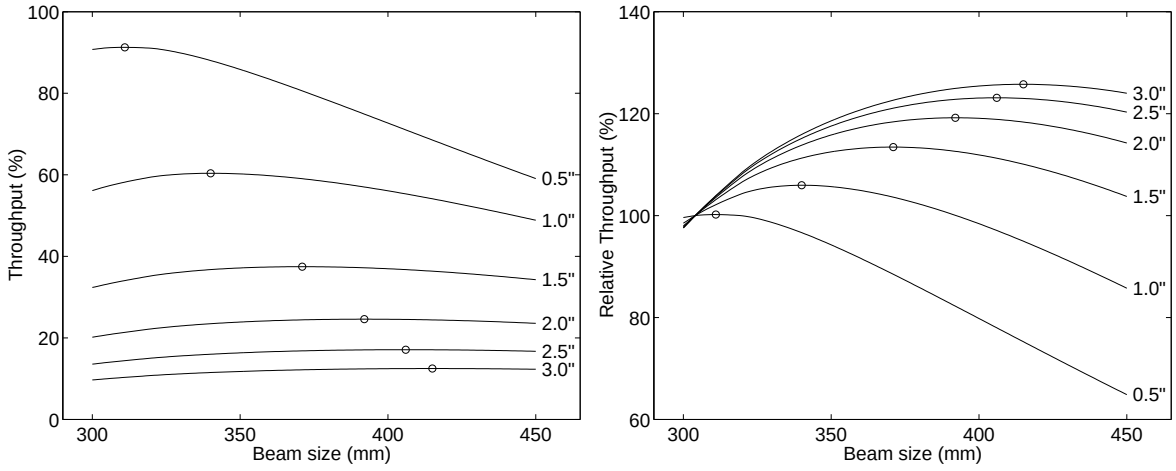

(a) Absolute efficiency (b) Relative efficiency

Figure 1.25: The absolute (a) and relative (b) efficiency for an R2 échelle grating with $W \times L = 300 \times 840$ for a resolving power of $R = 25\,000$ as a function of beam size and atmospheric seeing. Open circles indicate the most efficient beam size as a function of seeing.

Using such an analysis, for a given telescope and échelle grating combination, it is possible to choose an optimum beam size, where the weighting function would depend on the expected seeing conditions. A more detailed analysis would require that the effects of the secondary obstruction be considered (for directly fed spectrographs) and/or the effects of non-uniform illumination of the échelle grating (due, for instance, to the incomplete radial scrambling of the fibre far-field).

Blaze angle

As is shown in the following section, the choice of blaze angle will have little direct impact on the cross-dispersion. However, the blaze angle has a significant effect on the collimator and camera properties. These will be discussed in Section 1.2.3. For a further discussion of the choice of échelle grating blaze angle, and its implications on the spectrograph design, the reader is referred to Section **??** and to Hearnshaw et al. (1999).

Method of cross-dispersion

The amount of inter-order space can be tuned by altering the properties of the échelle grating. As shown above (equations 1.46 and 1.47) the inter-order spacing depends on the free spectral range of the échelle grating. That is, if the wavelength extent from one order to the next is increased, while the cross-dispersion remains constant, then the inter-order spacing will increase accordingly. Given that the free spectral range depends most sensitively on the grating groove spacing (equation 1.14), simply changing σ will change the inter-order spacing. If the échelle grating is more coarsely ruled (σ increased) then the free spectral range will increase, and therefore the total number of orders over a given wavelength range will decrease. The effect this will have on the spectral format is shown in Figure 1.26. One consequence of changing the échelle ruling density simply to increase the inter-order spacing is that the angular width of the orders also increases. This might be a problem if the angular field of view of the camera and detector is limited.

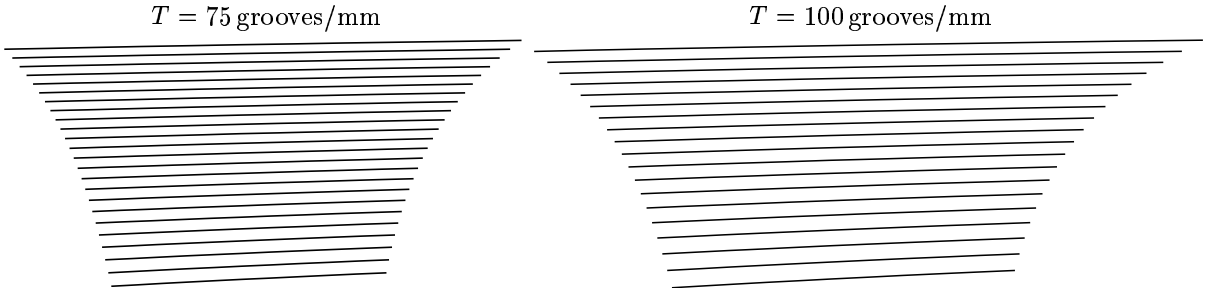

Figure 1.26: The effect of changing the échelle groove ruling density on order separation. The same (prism) cross-disperser and camera is used the two examples however the échelle groove spacing has changed as indicated.

Changing the blaze angle of the échelle grating has relatively little effect on the spectral format. That is, as discussed above in Section 1.1.9, the order separation Δy, for a given échelle and cross-disperser combination, is given by

$$\Delta y = \mathrm{Const.} \times \frac{1}{\sin\theta_{\mathrm{B}}} \quad , \tag{1.93}$$

(i.e., equations 1.47). Therefore, changing from an R2 grating to an R4 grating will decrease the order spacing by less than 10%. A description of the methods of cross-dispersion follows.

1.2.2 Cross dispersion

As has already being discussed, any combination of order number m and wavelength λ that satisfies the grating equation (equation 1.1) will have equal diffraction angles. If the wavelength coverage of interest spans more than a single free spectral range it will therefore be necessary to introduce dispersion in a direction that is orthogonal to the main échelle dispersion. Some possibilities for such cross-dispersion are discussed below.

Grating cross dispersion

The angular dispersion of a grating cross-disperser is

$$\frac{\mathrm{d}\beta}{\mathrm{d}\lambda}_{\mathrm{XD}} = \frac{m_{\mathrm{g}}}{\sigma_{\mathrm{g}} \cos\beta_{\mathrm{g}}} \quad , \tag{1.94}$$

where the grating order number m_{g} is generally low and the grating ruling density σ_{g} is high. Because the overall angular dispersion is quite low, the cross-disperser will be blazed at quite a shallow angle (i.e, β_{g} is small). The physical separation between orders is given by combining equation 1.94 with equation 1.47. That is,

$$\begin{aligned} \Delta y &= f_{\mathrm{cam}} \frac{m_{\mathrm{g}}}{\sigma_{\mathrm{g}} \cos\beta_{\mathrm{g}}} \frac{\lambda_{\mathrm{B}}^2}{2 \sin\theta_{\mathrm{B}} \cos\theta} \\ &= \mathrm{Const.} \times \lambda_{\mathrm{B}}^2 \quad . \end{aligned} \tag{1.95}$$

Prism cross dispersion

When using a prism for cross-dispersion the angle of incidence is usually such that the dispersed rays are very nearly parallel to the base of the prism (see Figure 1.27). While

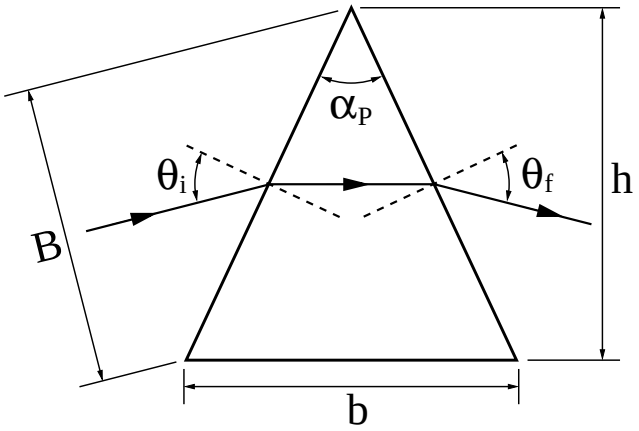

Figure 1.27: A prism used at minimum deviation.

this is close to the situation where a prism with a given apex angle has the least overall dispersion, this arrangement minimizes the total path length (of a wavelength which travels parallel to the base) and lessens the effects of polarization and reflection losses at

each face. The size of the prism is also minimized. The angular dispersion of a prism used near minimum deviation is given by

$$\frac{\mathrm{d}\beta}{\mathrm{d}\lambda_{\mathrm{XD}}} = \frac{b}{B}\frac{\mathrm{d}n}{\mathrm{d}\lambda} \quad , \tag{1.96}$$

where b is the length of the prism's base and B is the diameter of the incident beam. The ratio b/B effectively determines the prism apex angle α_{P}. That is,

$$\frac{b}{B} = \frac{\tan\theta_{\mathrm{i}}}{n_\lambda}\cot\frac{\alpha_{\mathrm{P}}}{2} \quad , \tag{1.97}$$

where θ_{i} is the angle of incidence of a wavelength (for which the prism refractive index is n_λ) such that

$$\sin\theta_{\mathrm{i}} = n_\lambda \sin\frac{\alpha_{\mathrm{P}}}{2} \quad . \tag{1.98}$$

This is the angle of incidence of a wavelength which has a minimum path length through the prism. Now, the refractive index of a prism can be approximated sing the Conrady formula by

$$n(\lambda) = k_1 + \frac{k_2}{\lambda^2} \quad , \tag{1.99}$$

where k_1 and k_2 are constants, and hence the angular dispersion of a prism is

$$\frac{\mathrm{d}\beta}{\mathrm{d}\lambda_{\mathrm{XD}}} = -2\frac{b}{B}\frac{k_2}{\lambda^3} \quad . \tag{1.100}$$

The separation between orders produced by a prism can be found by substituting Equation 1.100 into Equation 1.47 which gives

$$\begin{aligned} \Delta y &= -2f_{\mathrm{cam}}\frac{b}{B}\frac{k_2}{\lambda_{\mathrm{B}}^3}\frac{\lambda_{\mathrm{B}}^2}{2\sin\theta_{\mathrm{B}}\cos\theta} \\ &= \text{Const.} \times \frac{1}{\lambda_{\mathrm{B}}} \quad . \end{aligned} \tag{1.101}$$

Gratings or prisms?

The order separation for both prisms and gratings was derived above (equations 1.95 and 1.101). It was shown that the order separation was

$$\begin{aligned} \text{Gratings}: \quad \Delta y &= \text{Const.} \times \lambda_{\mathrm{B}}^2 \quad \text{and} \\ \text{Prisms}: \quad \Delta y &= \text{Const.} \times \frac{1}{\lambda_{\mathrm{B}}} \quad . \end{aligned}$$

This shows that the order separation given by a grating increases rapidly as the wavelength increases (i.e, as the square of the wavelength), while the order separation decreases (at a lesser rate) for a prism. This fact makes prisms particularly attractive in situations where it is desirable to capture a large wavelength range on a single detector. That is, if a prism and grating is chosen such that the total cross dispersion is the same (see Figure 1.28), the range of inter-order spacing of a grating will vary considerably. Generally this forces the design of an échelle spectrograph with grating cross-dispersion to incorporate several grating cross-dispersers so that the inter-order spacing at a chosen wavelength can

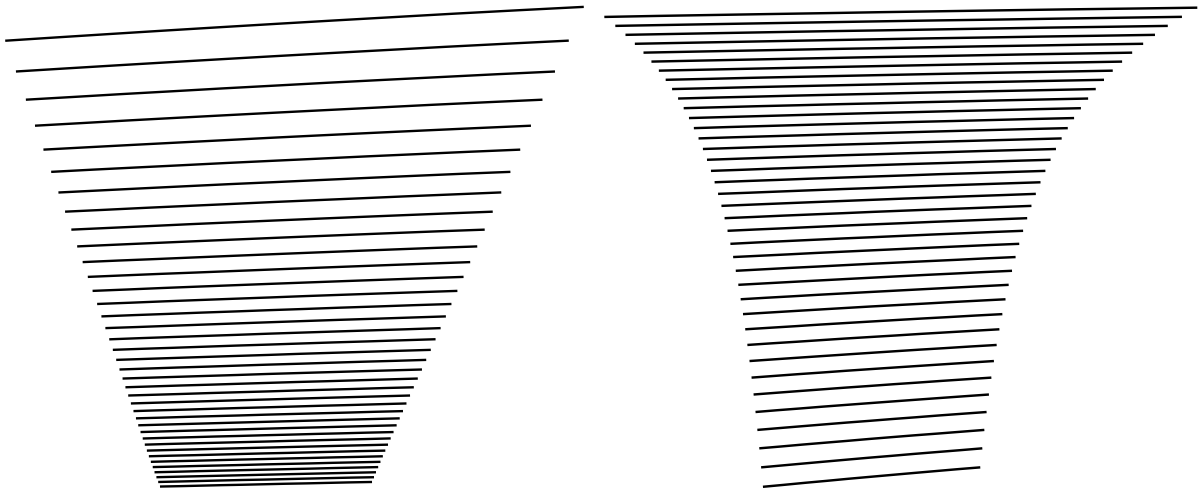

(a) Grating cross dispersion (b) Prism cross dispersion

Figure 1.28: The relative order separation of gratings (right) and prisms (left).

be varied. However, a prism has relatively uniform inter-order spacing, and one prism (or prismatic system) is sufficient for all wavelength regions. Alternatively, a combination of gratings and prisms (or a grism) could be considered.

Another aspect to consider is the relative efficiency of grating and prism cross-dispersers. It is generally the case that a high quality prism will have significantly higher efficiency over a broader wavelength range than any grating. This is because gratings are subject to the effects of the blaze function. A typical high efficiency surface relief grating will have a FWHM which is about equal to the blaze wavelength, and hence may only be considered useful over a small wavelength range. Recently however high efficiency gratings have been developed that have a periodic grating structure which arises from modulation of the index of refraction of a thin layer of light sensitive material. Such gratings are termed volume-phase holographic (VPH) gratings and are discussed further in Chapter **??**. These gratings cannot however be used over more than a single decade of spectral coverage and two or more gratings would still be required to cover a wavelength band spanning the near-UV to the near-IR (i.e., the approximate pass-band of a high efficiency CCD detector).

1.2.3 Collimator, camera and detector properties

Collimator

The required focal length of the collimator ($f_{\rm col}$) follows from the equality given by equation 1.23. That is,

$$f_{\rm col} = \frac{1}{\rho}\frac{f_{\rm tel}}{D}B \quad , \tag{1.102}$$

where the focal ration degradation factor $\rho = 1$ if the spectrograph is directly fed. The actual collimator focal length is a completely free parameter as long as the equality given by equation 1.23 is maintained.

Camera

The focal length of the camera $f_{\rm cam}$ is determined by noting that in order for the maximum resolving power $R_{\rm max}$ to be achieved the CCD must sample at least two resolution elements. It therefore follows that

$$f_{\rm cam} = \frac{n_{\rm samp}}{2} R_{\rm max} s_{\rm pix} \cot\theta_{\rm B} (1 + \tan\theta_{\rm B} \tan\theta) \quad , \tag{1.103}$$

where $n_{\rm samp}$ is the number of CCD pixels per resolution elements. Typically $n_{\rm samp} = 2$ for critical Nyquist sampling with pixels each having a size $s_{\rm pix}$, giving

$$f_{\rm cam} \simeq R_{\rm max} s_{\rm pix} \cot\theta_{\rm B} \quad , \tag{1.104}$$

for small θ. This shows that large blaze angle gratings require short focal length cameras. However, because $R = \text{Const.} \times B \tan\theta_{\rm B}$, (equation 1.58) the monochromatic focal ratio of the camera will be given by

$$\frac{f_{\rm cam}}{B} = \text{Const.} \times s_{\rm pix} \quad . \tag{1.105}$$

That it, for a given maximum attainable resolving power, the focal ratio of the spectrograph's camera will depend only on the CCD pixel size. The effective focal ratio of a spectrograph camera, which determines the camera's actual size, depends rather more on the location of the entrance pupil.

Detector

That the size of pixel chosen influences the camera's focal length and/or the was pointed out in the previous section. The number of pixels $n_{\rm pix}$ required by a detector to completely sample an order is given by

$$n_{\rm pix} = \frac{f_{\rm cam} \Delta\beta_{\rm FSR}}{s_{\rm pix}} \quad , \tag{1.106}$$

which, given equations 1.15 and 1.104, can be approximated to give

$$n_{\rm pix} \approx \frac{R_{\rm max} \lambda_{\rm B}}{\sigma \sin\theta_{\rm B}} \quad . \tag{1.107}$$

Given that $m\lambda_{\rm B} \approx 2\sigma \sin\theta_{\rm B}$, equation 1.107 can also be written as

$$n_{\rm pix} \approx \frac{2R_{\rm max}}{m} \quad , \tag{1.108}$$

which shows that all high resolution spectrographs require large detectors if wavelength coverage is complete. Often, for the sake of economy, compromises are made either in the maximum resolving power and/or wavelength coverage.

1.2.4 Fibres

The use of fibres in astronomy was first suggested by Angel et al. (1977). Their idea, which was made possible by the recent development of high quality fused silica fibres, was to link numerous small aperture telescopes to a single instrument. Subsequently

fibres were used in multi-fibre applications such as the simultaneous observation of many objects (for example, the Medusa spectrograph (Hill et al., 1980)), or to obtain spectra over a two-dimensional area (for example, the DensePax fibre optic array (Barden and Wade, 1988)). Both of these applications demonstrate that fibres contribute towards considerable improvements in the efficiency of spectroscopic observations.

Another practical benefit of the use of fibres is that the instrument is removed from the telescope. Hubbard et al. demonstrated the feasibility of this in 1979 (Hubbard et al., 1979). This removes the constraints of size and weight of any fibre-coupled instrument, while also allowing such an instrument to be placed in a potentially more stable environment, where the effects of flexure, temperature, and pressure changes may be absent. Hence fibres are of particular value for the high-precision measurement of radial velocities.

A further advantages of the use of fibres in precision spectroscopy is the ability of a fibre to scramble the input image structure. This means that regardless of the distribution of light on the input face of the fibre, the output face will appear more uniform. Hence, systematic errors due to slit illumination may be reduced. This type of image scrambling is referred to as "near-field" scrambling. It was also realized that the optics of a fibre-fed instrument may be illuminated more uniformly due to the scrambling properties of a fibre. That is, the angular distribution of rays exiting a fibre will not betray the distribution that entered the fibre. This type of "far-field" scrambling also has the potential to increase the stability of the spectrograph. However, as observed by Hunter and Ramsey (1992), and predicted by Heacox (1987), while the azimuthal scrambling of rays in the far field is nearly complete, the radial scrambling is not quite as good. These effects also impinge subtly on the illumination of the slit exit (or the "near-field" image) and hence may cause significant drifts in line profiles or positions. A method for increasing the scrambling via means of a "double-scrambler" has been proposed by Brown (1990). The double-scrambler is inserted in a break in the fibre and its purpose is to invert the positional and angular dependence of the rays crossing the junction between the two fibre halves.

The implications of coupling a spectrograph to a telescope via optical fibres was discussed above in Sections 1.1.6, 1.1.8, 1.1.10.

1.2.5 Merit functions

A common merit function used for comparing spectrographs is the slit-resolving power ($R\theta_{\rm s}$) product which follows from equation 1.61 (or equation 1.59). That is,

$$R\theta_{\rm s} = \frac{2L\sin\theta_{\rm B}\cos\theta}{\rho D} \quad . \tag{1.109}$$

As stated in Section 1.1.10, this equation shows that for a given resolving power and angular slit size, a large telescope requires a large grating. A more complete merit function would also take into account the throughput of the spectrograph, T; i.e., $TR\theta_{\rm s}$. This was introduced by Jacquinot (1954) in a different form. However, as pointed out by Vaughnn (1994), a more appropriate merit function would maximize the product of the signal-to-noise ratio (for each spectral element) and the total number of resolution elements. This is applicable because the performance of the spectrogragh is then intimately linked to the telescope and its environment.

Bibliography

Angel, J. R. P.; Adams, M. T.; Boroson, T. A. and Moore, R. L.: "A very large optical telescope array linked with fused silica fibers", *ApJ*, **218**, pp. 776–782, 1977 Dec.

Barden, S. C. and Wade, R. A.: "DensePak and spectral imaging with fiber optics", in "ASP Conf. Ser. 3: Fiber Optics in Astronomy", pp. 113–124, 1988.

Bingham, R. G.: "Grating spectrometers and spectrographs re-examined", *QJRAS*, **20**, pp. 395–421, 1979 Dec.

Bottema, M.: "Echelle efficiencies - theory and experiment; comment", *Appl. Opt.*, **20**, pp. 528–530, 1981 Feb.

Brown, T. M.: "High precision Doppler measurements via echelle spectroscopy", in "ASP Conf. Ser. 8: CCDs in astronomy", pp. 335–344, 1990.

Comte, A.: *Cours de Philosphie Positive*, chap. II, 19th lesson, 1835.

Diego, F. and Walker, D. D.: "On the possibility of increasing the throughput of astronomical spectrographs by overfilling the dispersing element", *MNRAS*, **217**, pp. 347–354, 1985 Nov.

Harrison, G. R.: "The production of diffraction gratings: I. the design of échelle gratings and spectrographs", *J. Opt. Soc. Am.*, **39**, pp. 522–528, 1949.

Harrison, G. R.; Loewen, E. G. and Wiley, R. S.: "Echelle gratings: their testing and improvement", *Appl. Opt.*, **15**, pp. 971–976, 1976 Apr.

Heacox, W. D.: "Radial image transfer by cylindrical, step-index optical waveguides", *Optical Society of America, Journal, A: Optics and Image Science (ISSN 0740-3232), vol. 4, March 1987, p. 488-493.*, **4**, pp. 488–493, 1987 Mar.

Hearnshaw, J.: *The analysis of starlight: one hundred and fifty years of astronomical spectroscopy*, Cambridge University Press, 1986.

Hearnshaw, J.; Rumsey, N. and Nankivell, G.: "Some comments on the design of échelle spectrographs using R2 or R4 gratings for precise radial velocity measurements", in "ASP Conf. Ser. 185: IAU Colloq. 170: Precise Stellar Radial Velocities", pp. 29–35, 1999.

Hill, J. M.; Angel, J. R. P.; Scott, J. S.; Lindley, D. and Hintzen, P.: "Multiple object spectroscopy - The Medusa spectrograph", *ApJ*, **242**, pp. L69–L72, 1980 Dec.

Hubbard, E. N.; Angel, J. R. P. and Gresham, M. S.: "Operation of a long fused silica fiber as a link between telescope and spectrograph", *ApJ*, **229**, pp. 1074–1078, 1979 May.

Huggins, W.: *The Nineteenth Century Review*, 1897 Jun.

Hunter, T. R. and Ramsey, L. W.: "Scrambling properties of optical fibers and the performance of a double scrambler", *PASP*, **104**, pp. 1244–1251, 1992 Dec.

Jacquinot, P.: "The lminosity of spectrometers with prisms, gratings, or Fabry-Perot etalons", *J. Opt. Soc. Am.*, **44**, pp. 761–765, 1954.

Kirchhoff, G. and Bunsen, R.: *Poggendorff's Ann.*, **110**, 1860.

Kitchin, C. J.: *Optical Astronomical Spectroscopy*, Institute of Physics Publishing, 1995.

Merrill, P. W.: "A Plane-Grating Spectrograph for the Red and Infra-Red Regions of Stellar Spectra", *ApJ*, **74**, pp. 188–+, 1931 Oct.

Michelson, A. A.: "The Echelon Spectroscope", *ApJ*, **8**, pp. 37–+, 1898 Jun.

Palmer and Verrill: "Diffraction gratings", *Contemp. Phys.*, **9**, pp. 257–276, 1968.

Palmer, C.: *Diffraction Grating Handbook*, Richardson Grating Laboratory, 2000.

Ramsey, L. W.: "Focal ratio degradation in optical fibers of astronomical interest", in S. C. Barden (ed.), "Fiber Optics in Astronomy, Astronomical Society of the Pacific Conference Series", vol. 3, pp. 26–40, 1988 Aug.

Schroeder, D. J.: "Echelle efficiencies - theory and experiment; author's reply to comment", *Appl. Opt.*, **20**, pp. 530–531, 1981 Feb.

Schroeder, D. J.: *Astronomical Optics*, Academic Press, 2nd ed., 2000.

Schroeder, D. J. and Hilliard, R. L.: "Echelle efficiencies - theory and experiment", *Appl. Opt.*, **19**, pp. 2833–2841, 1980 Aug.

Vaughnn, D.: "What's wrong with the throughput-resolution product? A fiber-fed spectrograph forces a

reevaluation of instrument design parameters", in "Proc. SPIE Vol. 2198, p. 31-43, Instrumentation in Astronomy VIII, David L. Crawford; Eric R. Craine; Eds.", vol. 2198, pp. 31–43, 1994 Jun.

Walker, D. D. and Diego, F.: "Design philosophy of the forthcoming echelle spectrographs for the AAT and LPO", *MNRAS*, **217**, pp. 355–365, 1985 Nov.

Wood, R. W.: "The échelette grating for the infra-red", *Phil. Mag.*, **20**, pp. 770–778, 1910.